[redacted]

ELECTRICAL

[redacted]

[redacted]

AUBURN RESEARCH FOUNDATI(

AUBURN UNIVERSITY

TECHNICAL REPORT NUMBER 3

THE DESIGN, CONSTRUCTION AND EVALUATION OF A CROSSED-SLOT, CAVITY BACKED ANTENNA

Prepared by

ANTENNA RESEARCH LABORATORY

E. R. GRAF, TECHNICAL DIRECTOR

April 19, 1965

CONTRACT NAS8-11251

GEORGE C. MARSHALL SPACE FLIGHT CENTER

NATIONAL AERONAUTICS AND SPACE ADMINISTRATION

HUNTSVILLE, ALABAMA

APPROVED BY

C. H. Weaver
Head Professor
Electrical Engineering

SUBMITTED BY

H. M. Summer
Project Leader

FOREWARD

This is a special technical report on a study conducted by the Electrical Engineering Department under the auspices of the Auburn Research Foundation toward the fulfillment of the requirements prescribed in NASA Contract NAS8-11251. An evaluation of a crossed-slot, cavity backed antenna element having application as an element in an electronically scanned array is presented.

ABSTRACT

The present trend in tracking antennas is toward electronically scanned arrays. These arrays consist of a number of antenna elements. The phase or amplitude is varied between these elements to point the beam of the antenna to a position in space without a mechanical movement of the antenna structure. The slot antenna is applicable to the electronically scanned antenna array.

A theoretical discussion of the electromagnetic field characteristics of a crossed-slot antenna is presented through the application of Babinet's Principle to the dipole antenna.

The antenna has a theoretical elevation pattern which is a hemisphere. This is true only when the antenna is constructed in an infinite ground plane. The crossed-slot antenna has elliptical polarization when the slots are excited with a signal of the proper amplitude and phase. The design of a resonant cavity to fulfill these conditions is discussed.

Two test antennas were constructed. Each antenna is fed with a resonant cavity which has two coupling loops. These loops are magnetically coupled to the cavity at a magnetic field maximum. The difference between the test antennas is that one has been reduced in mechanical size through the use of dielectric loading.

Antenna patterns for the two test antennas are presented.

The antennas exhibit elliptical polarization and a broad beamwidth in the θ plane

TABLE OF CONTENTS

LIST OF TABLES

LIST OF FIGURES

I. INTRODUCTION

A need exists for improvements in tracking antennas designed to be used in conjunction with space vehicles and artificial earth satellites. Such an antenna must have a relatively narrow beam width. The beam also must be scannable in order to follow the path of a space vehicle. Large parabolic reflectors have been used for this purpose. The motion of the antenna is controlled by a servomechanism system and the beam moves as the antenna position is changed. This has the disadvantage of requiring a large mass to be moved by a motor. In addition, it is often necessary that an operator be present when the antenna is functioning.

Lately, electronic scanning antennas have been used successfully. In these the physical antenna remains stationary while the beam is moved by electronic means. The antenna consists of a number of elements. The beam is moved by varying quantities such as the phase or amplitude between the individual elements.

These elements are usually identical. The final pattern of the antenna is the multiplication of the pattern of each individual element and that of the configuration or array in which these elements are located.

In order to move the beam through a hemisphere of coverage the pattern of the individual element should be as nearly hemispherical

as possible. This prevents nulls from occurring in the final pattern of the antenna as the beam is scanned.

The antenna should have elliptical polarization because of the changing relative orientation of the vehicle transmitting antenna. Elliptical polarization enables the antenna to track regardless of the orientation of the vehicle.

The crossed-slot, cavity backed antenna ideally has these desired characteristics. In addition it has a physical advantage due to its shape. The radiating portion of the slot antenna is a flat plate in which slots are cut. This allows the entire antenna to be mounted internally with the radiating portion flush with the surface of the mounting structure. This configuration is quite desirable for the type of antenna application in question.

II. THEORETICAL DISCUSSION

The slot antenna

The slot antenna may consist simply of a narrow cut in a flat sheet of conducting material. The spatial orientation of the electromagnetic field in the slot does not generally depend on the spatial orientation of the electromagnetic field in the feed structure. The field in the slot is determined by the boundary conditions for the conductor containing the slot. The boundary conditions are

$$\bar{n} \times \bar{E} = 0 \tag{1}$$

and

$$\bar{n} \cdot \bar{B} = 0, \tag{2}$$

where $\bar{n}$ is a unit vector everywhere normal to the conductor in which the slot is cut, $\bar{E}$ the electric field vector, and $\bar{B} = \mu\bar{H}$ the magnetic vector. Thus, the electric field must be everywhere perpendicular to the surface in which the slot is cut.

The field in the slot has the configuration shown in Figure 1, with the line density representing electric field magnitude. The electric field tangent to the slot ends must be zero to satisfy the boundary conditions. In the case of a resonant slot antenna ($\lambda/2$ in length) the $\bar{E}$ field will have a distribution of approximately

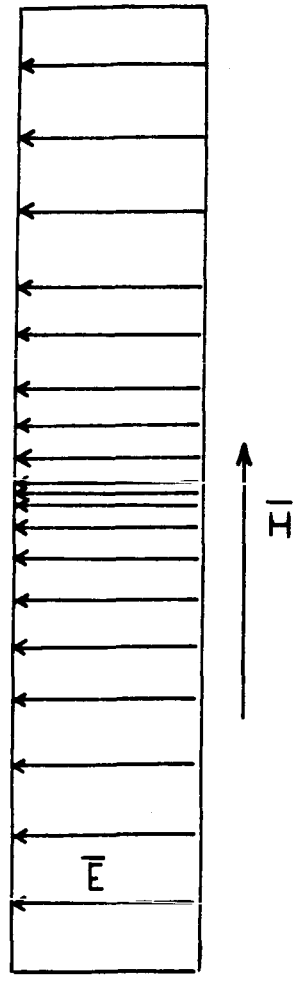

Fig. 1--The Electric Field Variation in a Slot Antenna

$$E = E_{max.} \cos k\ell, \tag{3}$$

where ℓ is measured in wavelengths from the center to the ends of the slot and $k = 2\pi/\lambda$.

This field configuration is seen to be the exact complement of an electric dipole with the electric and magnetic fields interchanged. This is known as the duality principle and is stated as follows:

> If an e.m.f. of frequency f is applied to an ideal slot antenna from an arbitrary source, the electromagnetic field vectors $\bar{E}$ and $\bar{H}$ in the slot and the space surrounding the slot will have the same directions and will be the same functions of the space co-ordinates as the directions and the functions of the vectors $\bar{H}$ and $\bar{E}$ respectively of the field of a dipole consisting of an ideally conducting infinitely thin plate, located in free space and having the same shape and dimensions as the slot, when an e.m.f. of the same frequency f is applied to the plate at corresponding points.[1]

This corresponds to the Babinet principle in optics which states:

> The field at any point behind a plane having a screen, if added to the field at the same point when the complementary screen is substituted, is equal to the field at the point when no screen is present.[2]

Thus,

$$U_o'(P) + U_o''(P) = U_o(P), \tag{4}$$

where $U_o(P)$ is the unobstructed amplitude at a point P and $U_o'(P) + U_o''(P)$ is the amplitude at point P due to the screen plus its complement.

The patterns in the radiation field and the near zone may be de-

rived from those of a complementary dipole antenna. The radiation conductance, g_1, of the slot is related to that of the complementary dipole by

$$g_1 = \frac{R_\epsilon}{(60\pi)^2} \tag{5}$$

where R_ϵ is the radiation resistance of the dipole.[1] The admittance, Y_1, of the slot is

$$Y_1 = \frac{1}{(60\pi)^2} (R_\epsilon + jX_2), \tag{6}$$

where X_2 is the reactive component of the complementary dipole.

Radiation field patterns of a slot antenna

Consider the co-ordinate system of Figure 2. Let a short dipole of length $\Delta\ell$ be oriented along the z-axis with the center at the origin. The vector potential at a field point P is

$$\overline{A} = \int_c \frac{\mu I \overline{d\ell}}{4\pi r}, \tag{7}$$

where c denotes the current carrying path and I is the current carried by an element of length $d\ell$. In the co-ordinate system pictured $\overline{d\ell}$ has only a z component and the vector potential is

$$A_z = \frac{\mu}{4\pi} \int_{-\Delta\ell/2}^{\Delta\ell/2} \frac{[I]}{s} dz \tag{8}$$

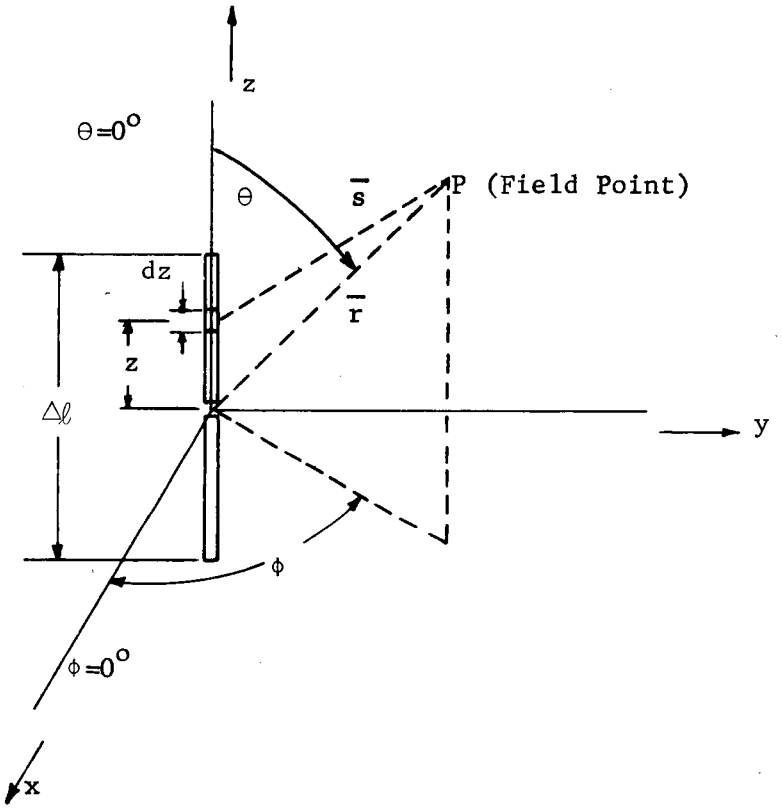

Fig. 2--The Cocrdinate System Showing the Orientation of a Very Short Dipole

where $\Delta\ell$ is the length of a small antenna situated along the z-axis, s is the distance from the current element to the field point and $[I]$ is the retarded current. The retarded current is

$$I = I_o e^{j\omega(t-s/c)}, \tag{9}$$

where $\omega = 2\pi f$. For the short dipole, s may be approximated by r and held constant in the integration. The integrand is constant and the vector potential becomes

$$A_z = \frac{\mu \ell I_o e^{j\omega(t-r/c)}}{4\pi r} \tag{10}$$

The magnetic field, $\overline{H}$, is found from the relation,

$$\overline{H} = \frac{1}{\mu} \nabla \times \overline{A} . \tag{11}$$

In terms of the coordinate system depicted on Figure 2, $\overline{H}$ may be written

$$\overline{H} = H\overline{a}_\phi = \frac{I_o \ell \sin\theta e^{j\omega(t-r/c)}}{4\pi} \left(\frac{j\omega}{rc} + \frac{1}{r^2} \right) \overline{a}_\phi, \tag{12}$$

where $\overline{a}_\phi$ is a unit vector in the ϕ direction. In the far field, only the term containing $\frac{1}{rc}$ is of importance; therefore

$$H_\phi = \frac{I_o \ell \sin\theta}{2\lambda r} e^{j\omega(t-r/c)}. \tag{13}$$

Consider a dipole of length $\lambda/2$ composed of these short dipoles. Associated with an element of length dz of this dipole is a magnetic field, dH_ϕ,

$$dH_\phi = \frac{j [I] \sin\theta dz}{2\lambda s}, \tag{14}$$

where $dH_\phi = H_\phi$ of the short dipole considered previously. The current I_ℓ for a dipole of length L is[4]

$$I_\ell = I_o \sin \left[\frac{2\pi}{\lambda} \left(\frac{L}{2} \pm z \right) \right] e^{j\omega(t-s/c)}, \tag{15}$$

For the particular case that L is one half of a wavelength λ, i.e., $L = \lambda/2$,

$$I_{\lambda/2} = I_o \sin\left[\frac{\pi}{2} \pm z \right] e^{j\omega(t-s/c)}. \tag{16}$$

For the $\lambda/2$ dipole $s \approx r$. The path, s, is dependent upon z in Figure (2) and must now be considered in the integral. Figure 3 depicts the geometry for the required integration. One may see from the geometry that

$$s = r - z \cos\theta. \tag{17}$$

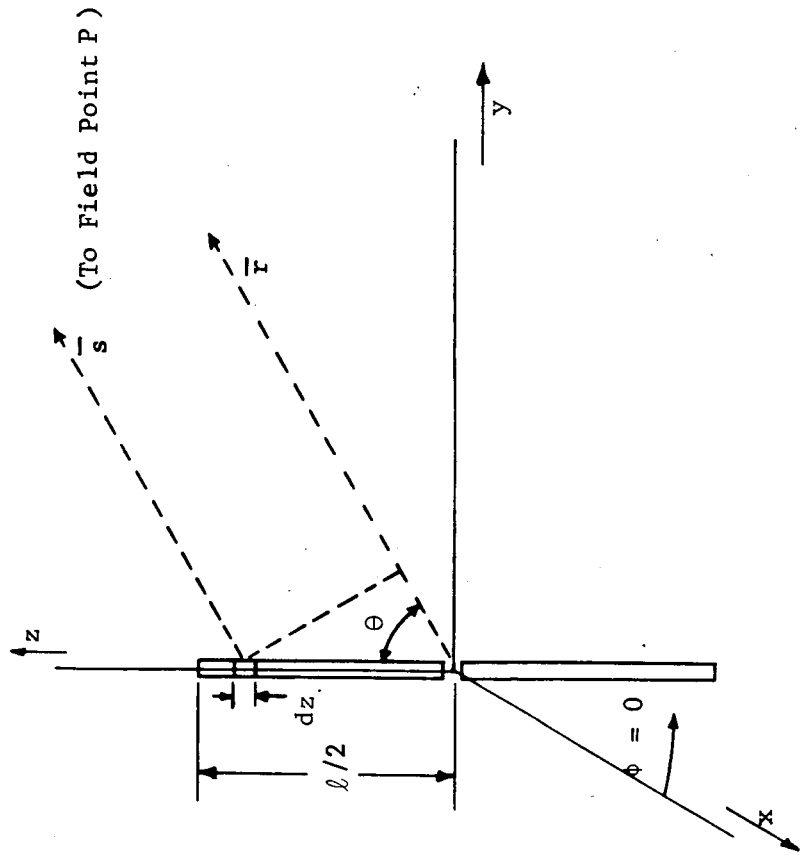

Fig. 3--The Coordinate System Showing the Orientation of a Dipole λ/2 in Length

The total magnetic field is obtained from the integration of the magnetic fields of the infinitesimal dipoles of length dz, or

$$H_\phi = \int_{-L/2}^{L/2} dH_\phi . \tag{18}$$

For the particular case of a dipole of length $\lambda/2$, equation (18) may be integrated to obtain

$$H_\phi = \frac{j \left[I_o\right] \cos(\frac{\pi}{2}\cos\theta)}{2\pi r \sin\theta} . \tag{19}$$

The electric field for the slot antenna is found by the application of Babinet's Principle to be

$$E_\phi = \frac{j \left[I_o\right] \cos(\frac{\pi}{2}\cos\theta)}{2\pi r \sin\theta} , \tag{20}$$

when the slot is oriented in the manner of the dipole in Figure 2. It must be remembered, however, that the dipole existed in free space. Thus, the slot antenna must be the complement of the dipole and exist in an infinite ground for equation (20) to hold exactly. For an infinite ground plane, the pattern in the xy plane of Figure 3 is omnidirectional for the slot and varies as the pattern factor

$$\frac{\cos(\frac{\pi}{2}\cos\theta)}{\sin\theta} \tag{21}$$

in the yz plane. The radiation patterns for this ideal case are shown in Figure 4. The radiation is equal from the two sides of the ground plane, but the phase of the radiation field is reversed from one side to the other.

Consider the radiation from one side of the conducting sheet. The hemispherical pattern in the ϕ-plane is obtained only for an infinite ground plane. The pattern of the slot is dependent upon the current distribution on the conducting ground plane. The current distribution changes with an alteration in ground plane configuration or size; therefore, the ϕ plane pattern will be changed under these conditions. Several methods are available for approximate calculation of the radiation field of a slot in a finite ground plane, but these are lengthy and give results that are difficult to correlate with experimental data. Jasik[3] gives measured examples of ϕ patterns for various ground plane sizes. These patterns are shown in Figure 5. The θ plane pattern is relatively unaffected by changes in ground plane size.

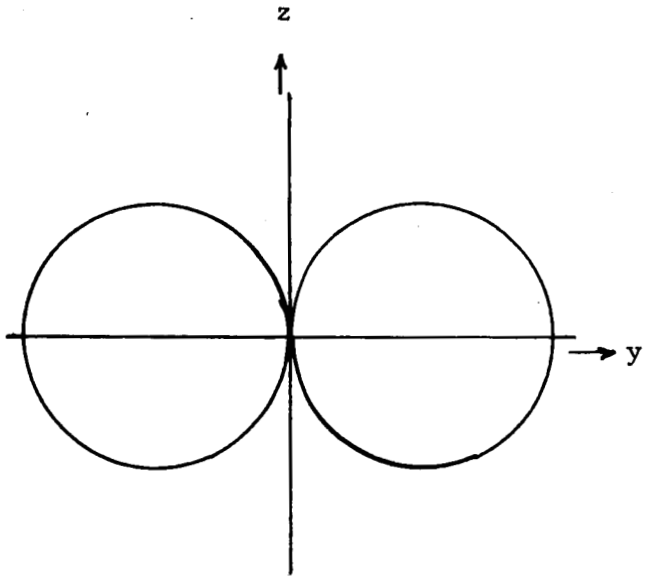

Θ Plane Pattern

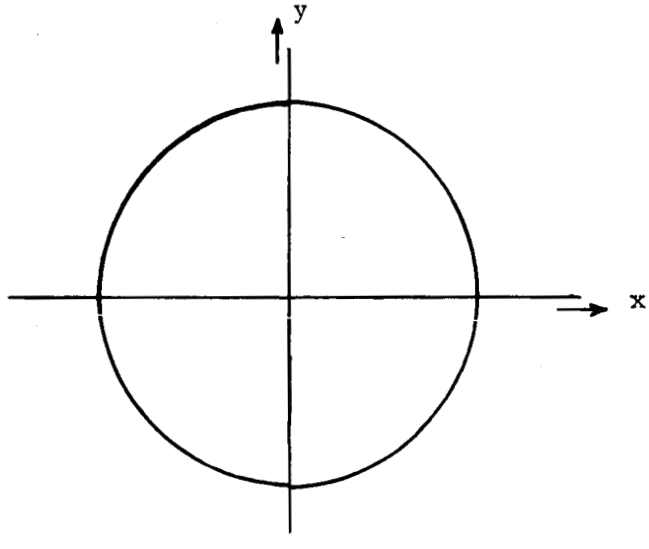

Φ Plane Pattern

Fig. 4--The Θ and Φ Plane Patterns of a Slot Antenna in An Infinite Ground Plane Oriented as in Figure 3.

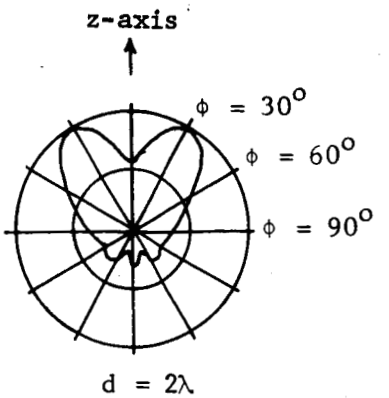

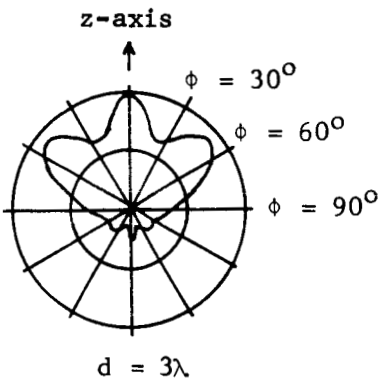

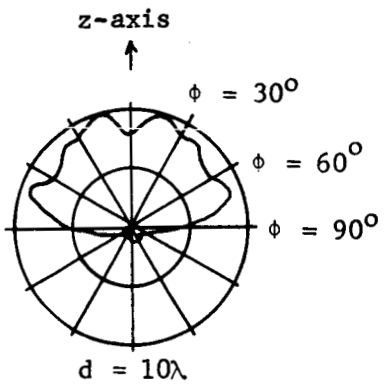

Fig. 5--Polar Plots of the ϕ Plane Pattern for Various Ground Plane Diameters (d)

Radiation patterns and polarization of a crossed slot antenna

Consider two dipoles of length $\ell/2$ oriented as shown in the coordinate system of Figure 6. The patterns of each dipole may be obtained by a rotation of the coordinate system of Figure 3 and transformation of the equations obtained for a dipole in this coordinate system. In the coordinate system of Figure 3, $\bar{H} = H_\phi \bar{a_\phi}$, or

$$\bar{H} = \frac{\cos(\frac{\pi}{2}\cos\theta)}{\sin\theta}\left[- \sin\phi\ \bar{a_x} + \cos\phi \bar{a_y}\right], \tag{22}$$

where $\bar{a_x}$ and $\bar{a_y}$ are unit vectors along the x-axis and y-axis. In this coordinate system $\cos\theta = \frac{z}{r}$, $\sin\theta = \frac{\sqrt{x^2 + y^2}}{r}$, $\sin\phi = \frac{y}{\sqrt{x^2 + y^2}}$ and $\cos\phi = \frac{x}{\sqrt{x^2 + y^2}}$.

One may substitute the above relations into equation (22) to obtain

$$\bar{H} = \frac{\cos(\frac{\pi}{2}\frac{z}{r})}{\sqrt{\frac{x^2 + y^2}{r}}}\left[\frac{- y\bar{a}_x}{\sqrt{x^2 + y^2}} + \frac{x\bar{a}_y}{\sqrt{x^2 + y^2}}\right]. \tag{23}$$

Let the coordinate system be rotated in a clockwise direction about the y axis and the new axes denoted by x', y' and z'. The following relations hold: $x = z'$, $y = y'$, $z = x'$ and $r = r'$.

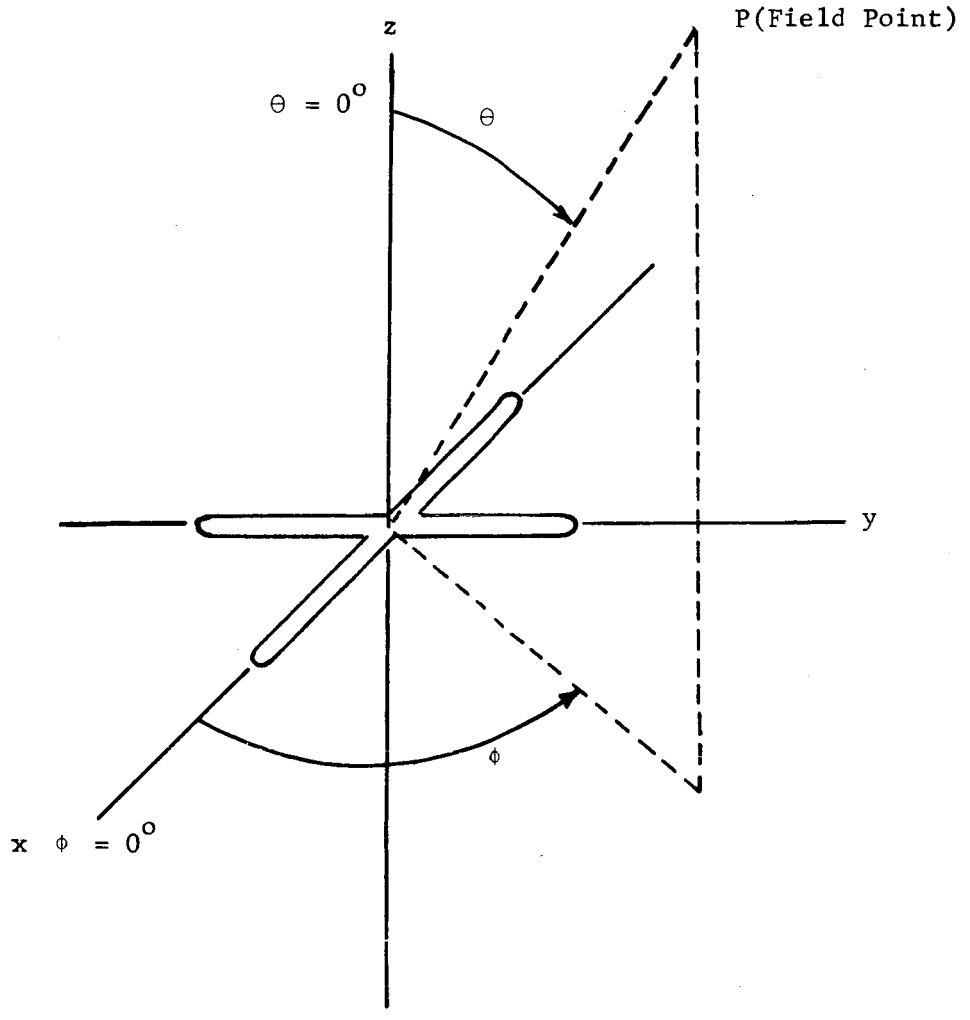

Fig. 6--The Coordinate System Showing the Orientation of the Crossed-Slot Antenna

In the rotated coordinate system

$$\overline{H} = \frac{\cos\left(\frac{\pi}{2}\frac{x'}{r}\right)}{\frac{(z')^2+(y')^2}{(r')^2}}\left[\frac{-y'\overline{a_z}}{r'} - \frac{z'\overline{a_y}}{r'}\right]. \tag{24}$$

The quantity $\frac{x'}{r'}$ is the direction cosine between the x' axis and the vector r'. The direction cosines $\frac{x'}{r'}$ and $\frac{y'}{r'}$ are related to θ' and ϕ' by

$$\frac{x'}{r'} = \sin\theta'\cos\phi' \tag{25}$$

and

$$\frac{y'}{r'} = \sin\theta'\sin\phi'. \tag{26}$$

Since

$$\frac{z'^2 + y'^2}{(r')^2} = 1 - \sin^2\theta\cos^2\phi, \tag{27}$$

one may substitute equations (25),(26) and (27) into equation (24) to obtain the expression

$$\overline{H} = \frac{\cos\left(\frac{\pi}{2}\sin\theta\cos\phi\right)}{1 - \sin^2\theta\cos^2\phi}\left[\sin\theta\sin\phi\ \overline{a_z} - \cos\theta\overline{a_y}\right] \tag{28}$$

The magnetic field component in the θ direction due to the x axis dipole is obtained by computing the scalar product $\overline{H} \cdot \overline{a_\theta}$.

The ϕ and r components, $H_{\phi x}$ and H_{rx} due to the x axis dipole are obtained in a similar manner. The H_r component is equal to zero if either the x axis or the y axis coincides with the axis of the dipole. The normalized magnetic field components in the radiation field are:

$$H_{\theta x} = \frac{\sin\phi\cos(\frac{\pi}{2}\sin\theta\cos\phi)}{1 - \sin^2\theta\cos^2\phi} \tag{29}$$

and

$$H_{\phi x} = \frac{\cos\theta\cos\phi\cos(\frac{\pi}{2}\sin\theta\cos\phi)}{1 - \sin^2\theta\cos^2\phi} \tag{30}$$

when the dipole is aligned along the x-axis and,

$$H_{\theta y} = \frac{\cos\phi\cos(\frac{\pi}{2}\sin\theta\sin\phi)}{1 - \sin^2\theta\sin^2\phi} \tag{31}$$

and

$$H_{\phi y} = \frac{\cos\theta\sin\phi\cos(\frac{\pi}{2}\sin\theta\sin\phi)}{1 - \sin^2\theta\sin^2\phi} \tag{32}$$

for alignment of the dipole along the y-axis.

The electric field of the complementary slot antennas is obtained by the application of the duality principle. The normalized electric field components in the radiation field are

$$E_{\theta x} = \frac{\sin\phi\cos(\frac{\pi}{2}\sin\theta\cos\phi)}{1 - \sin^2\theta\cos^2\phi} \tag{33}$$

and

$$E_{\phi x} = \frac{\cos\theta\cos\phi\cos(\frac{\pi}{2}\sin\theta\cos\phi)}{1 - \sin^2\theta\cos^2\phi} \tag{34}$$

for a complementary slot along the x-axis with the center at the origin, and

$$E_{\theta y} = \frac{\cos\phi\cos(\frac{\pi}{2}\sin\theta\sin\phi)}{1 - \sin^2\theta\sin^2\phi} \tag{35}$$

and

$$E_{\phi y} = \frac{\cos\theta\sin\phi\cos(\frac{\pi}{2}\sin\theta\sin\phi)}{1 - \sin^2\theta\sin^2\phi} \tag{36}$$

for a complementary slot along the y-axis

A crossed slot antenna oriented as in the coordinate system of Figure 6 will have a normalized electric field intensity pattern obtained by the vector addition of the normalized electric field intensity patterns of the two perpendicular slots.

The θ component of the electric field for the crossed slot antenna of Figure 6 is obtained by the addition of the θ components of each slot. It may be expressed as

$$E_\theta = E_{\theta x} - jE_{\theta y}\ , \tag{37}$$

where the negative sign is used to indicate a time difference, (in this case a lag of the y-axis field component behind the x-axis field

component) between the two components. This is the condition for right-hand elliptical polarization.[4] Equation (37) may be rewritten as

$$E_\theta = \frac{\sin\phi\cos(\frac{\pi}{2}\sin\theta\cos\phi)}{1 - \sin^2\theta\cos^2\phi} - j\frac{\cos\phi\cos(\frac{\pi}{2}\sin\theta\sin\phi)}{1 - \sin^2\theta\sin^2\phi} \quad . \tag{38}$$

The ϕ component of the electric field may be treated in a similar manner to obtain

$$E_\phi = E_{\phi x} - jE_{\phi y} \, , \tag{39}$$

or

$$E_\phi = \frac{\cos\theta\cos\phi\cos(\frac{\pi}{2}\sin\theta\cos\phi)}{1 - \sin^2\theta\cos^2\phi} - j\frac{\cos\theta\cos\phi\cos(\frac{\pi}{2}\sin\theta\cos\phi)}{1 - \sin^2\theta\sin^2\phi} \quad . \tag{40}$$

Equations (38) and (40) are the pattern factors for the E_θ and E_ϕ components for the crossed-slot antenna. Plots of these factors show the θ component to be present throughout the hemisphere and have only a variation of 1 decibel from the maximum value for an infinite ground plane. Figure 7 shows the normalized field pattern for the θ component in the plane of maximum variation, i.e., $\phi = 45^\circ$. This figure also shows the normalized field pattern for the ϕ component in this plane as a function of the angle θ.[5]

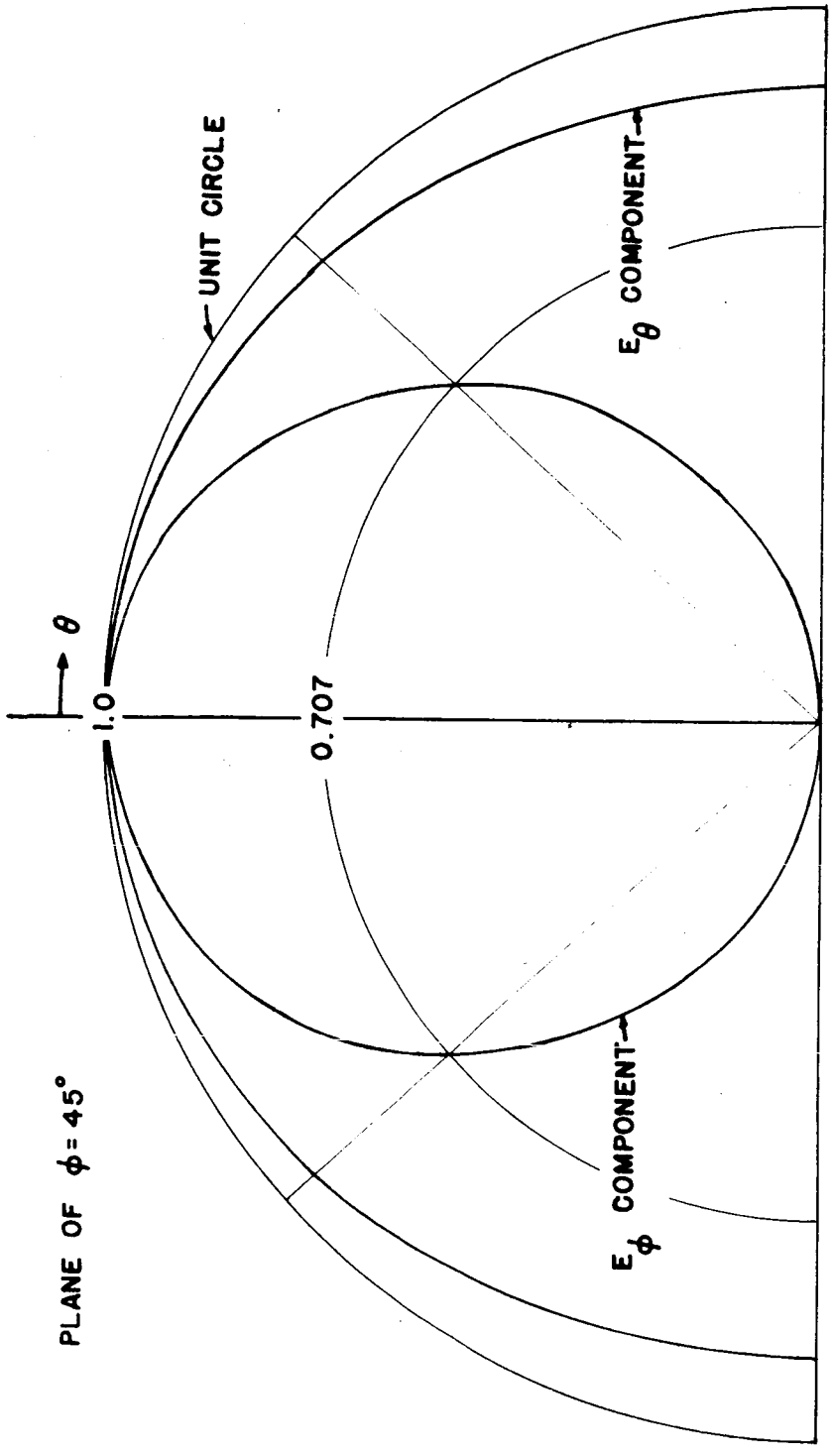

Fig. 7--The Normalized field Pattern of the Crossed Slot Antenna in the Plane of the Maximum Variation of the E_Θ - Component.

Cavity consideration for feeding the crossed slot antenna

The polarization of an electric wave is defined as the orientation of the electric field vector during one full cycle of the wave. Generally, the magnitude and phase of the vector vary and describe an ellipse in a plane perpendicular to the direction of propagation. At any time t, this ellipse may be investigated. The polarization will appear as a vector of a certain magnitude at a phase angle in the plane. This in turn may be broken down into orthogonal components. These are:

$$E_x = E_1 \cos\omega(t - \frac{z}{v}) \tag{41}$$

and

$$E_y = E_2 \cos\left[\omega(t - \frac{z}{v}) + \psi\right], \tag{42}$$

where E_1 and E_2 are the magnitudes of the x and y components, z is the direction of propagation, v is the velocity of propagation and ψ some phase angle. In the plane, $z = 0$, we have

$$E_x = E_1 \cos\omega t \tag{43}$$

and

$$E_y = E_2 \cos(\omega t + \psi) \ . \tag{44}$$

The last two equations are seen to be the parametric equations for an ellipse if $\psi = \pi/2$. Thus an elliptically polarized wave may be considered as the resultant of two linearly polarized waves of the same frequency.

If $E_1 = E_2$ and $\psi = \frac{\pi}{2}$ the resultant obtained by adding the E_x and E_y components will always describe a circle. If $\psi = \pi/2$ the resultant vector rotates in a counterclockwise direction when viewed in the direction of propagation. This is said to be left-hand circular polarization. If $\psi = -\frac{\pi}{2}$ the vector rotates clockwise and is said to be right-hand circular polarization.

The conditions for circular polarization are that there be two orthogonal electric vectors of equal magnitude with a time phase shift of $\pi/2$ between them.[6] Thus a circularly polarized antenna may be constructed from two identical linear polarized antennas orthogonal in space

Design of the resonant cavity

The cavity feed for the slot antenna may be viewed as a section of waveguide terminated by two conducting plates. Maxwell's equations must satisfy the boundary conditions imposed by the conducting walls of the cavity. The equations have many solutions and each of these is called a "mode" of the waveguide.

Consider the waveguide section of Figure 8. If one assumes the waveguide walls to be ideal conductors it is possible to solve for the transverse electric and magnetic field components: i.e.; E_x, E_y, H_x, and H_y, in terms of the axial components, H_z and E_z.

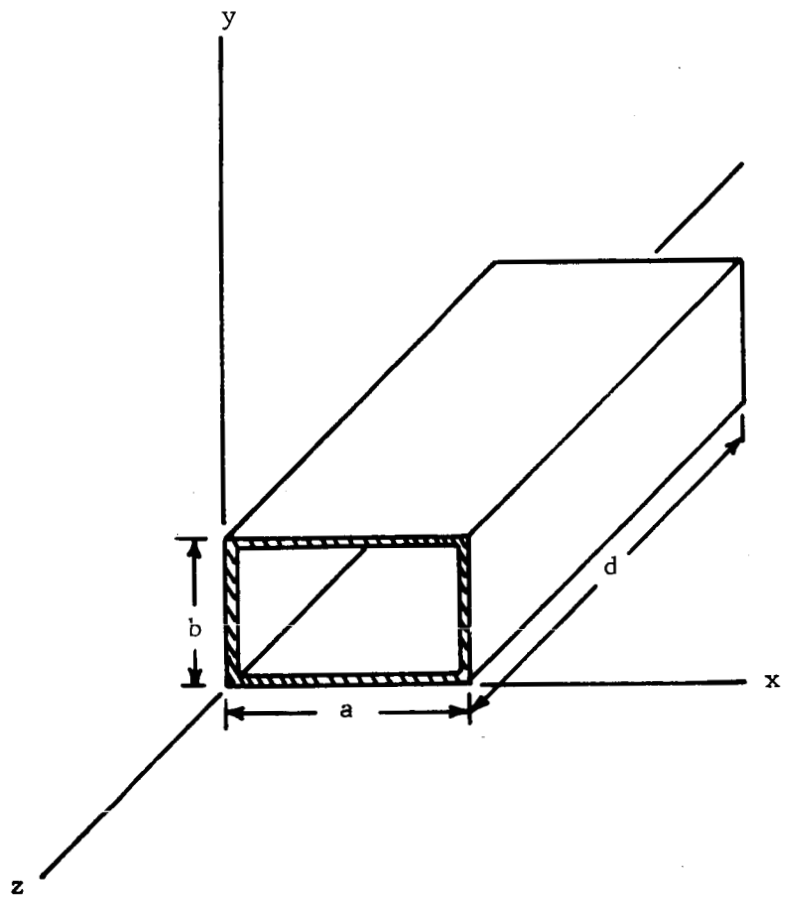

Fig. 8--The Coordinate System Showing the Orientation of a Rectangular Waveguide Section

For the transverse electric mode, i.e., the one in which there is no longitudinal electric field component, the field equations are given by Ramo and Whinney[6] as

$$H_z = B\cos K_x X \cos K_y Y, \tag{45}$$

where B is a constant, and

$$E_z = 0. \tag{46}$$

The quantities X and Y give the distance along the sides a and b respectively and

$$K_x = \frac{m\pi}{a}$$

and $$m, n = 1, 2, 3 \ldots \tag{47}$$

$$K_y = \frac{n\pi}{b} .$$

The positive integers m, n denote the waveguide mode or the particular solution of Maxwell's equations being considered.

The transverse components are

$$E_x = \frac{j\omega\mu}{K_c^2} K_y B\cos K_x X \sin K_y Y, \tag{48}$$

$$E_y = \frac{-j\omega\mu}{K_c^2} K_y B\sin K_x X \cos K_y Y, \tag{49}$$

$$H_x = -\frac{\gamma}{K_c^2} K_x B \sin K_x X \cos K_y Y \tag{50}$$

and

$$H_y = \frac{\gamma}{K_c^2} K_y B \cos K_x X \sin K_y Y, \tag{51}$$

where $K_c = K_x + K_y$ and $\gamma^2 = K_c^2 - K^2$ is the propagation constant which determines the z dependence of the field component, i.e.,

$$E \sim e^{-\gamma z} \tag{52}$$

and

$$H \sim e^{-\gamma z}. \tag{53}$$

If γ is real the wave is attenuated as it travels. If γ is imaginary the wave is not attenuated. If $\gamma = 0$ the wave is at what is designated cut-off with a wavelength defined by

$$\lambda_c = \frac{v}{f_c} = \frac{2\pi}{K_c}. \tag{54}$$

The propagation constant γ has both a real and imaginary part, i.e.,

$$\gamma = \alpha + j\beta. \tag{55}$$

When the waveguide is above cut-off $\gamma = j\beta$ and

$$\beta = \sqrt{K^2 - K_c^2} = K\sqrt{1 - K_c^2/K^2} \quad . \tag{56}$$

One may substitute the values of K_c and K into equation (56)

$$\beta = K\sqrt{1 - (\lambda/\lambda c)^2} \quad . \tag{57}$$

The waveguide wavelength, λ_g, is the distance in which the phase of the field component proportional to $e^{-j\beta z}$ increases by 2π or

$$\lambda_g = \frac{2\pi}{\beta} \quad , \tag{58}$$

which may be expressed as

$$\lambda_g = \frac{\lambda}{\sqrt{1 - (\lambda/\lambda c)^2}} \quad . \tag{59}$$

It may be seen from equation (59) that above cut-off the waveguide wavelength is greater then the free space wavelength λ.

For the waveguide to be a resonant cavity conducting plates are placed on each end at a distance

$$d = \frac{\ell\lambda_g}{2}, \qquad \text{where} \qquad \ell = 1, 2, 3 \ldots \quad . \tag{60}$$

The length of a resonant cavity is

$$d = \frac{\lambda \ell}{2\sqrt{1 - (\lambda/\lambda c)^2}} \quad . \tag{61}$$

Equation (61) may be solved for λ which yields

$$\frac{1}{\lambda^2} = \left(\frac{\ell}{2d}\right)^2 + \frac{1}{\lambda c^2} \quad . \tag{62}$$

Equation (62) may be used to determine the allowed wavelength in the cavity and therefore the resonant frequency of the cavity.

A traveling wave may be represented as the sum of two waves propagating in opposite directions, i.e.,

$$E = A(E^+ e^{-\gamma z} + E^- e^{\gamma z}) \tag{63}$$

or for the case of lossless transmission

$$E = A(E^+ e^{-j\beta z} + E^- e^{j\beta z}) \quad . \tag{64}$$

The magnetic field component must satisfy the Maxwell equation

$$\overline{H} = -\frac{1}{j\omega\mu} \nabla \times \overline{E} \quad . \tag{65}$$

If only an E_x component is assumed to be present in the cavity

$$\bar{H} = \bar{a}_y \frac{1}{j\omega\mu} \frac{\partial E_x}{\partial z} . \tag{66}$$

For a wave, E^+, traveling in the positive z direction $E^+ = Ae^{-j\beta z}$, where A is an amplitude constant which is a function of the boundary conditions on the waveguide sidewalls. Equation (66) may be solved for H_y^+, the H_y component in the positive z direction. This procedure yields

$$H_y^+ = \frac{-1}{j\omega\mu} \frac{\partial}{\partial z} (Ae^{-j\beta z}) = \frac{A}{Z} e^{-j\beta z} , \tag{67}$$

where

$Z = \frac{j\omega\mu}{\gamma} = \frac{j\omega\mu}{\beta}$. Similarly, the negative traveling wave, H_y^-, is

$$H_y^- = - \frac{1}{j\omega\mu} \frac{\partial}{\partial z} (Ae^{j\beta z}) = - \frac{A}{Z} e^{j\beta z} . \tag{68}$$

The tangential electric field must be equal to zero at the cavity shorting plate; hence,

$$E_x^+ + E_x^- = 0 \tag{89}$$

Therefore, $E_x^+ = - E_x^-$ and $H_y^- = \frac{A}{Z} e^{j\beta z}$. The electric and magnetic field components obtained from (64) are

$$E_x = - 2jA\sin\beta z \tag{70}$$

and

$$H_y = \frac{2A}{Z} \cos\beta z \ . \tag{71}$$

Therefore, the electric and magnetic fields have a time phase difference of $\pi/2$ and a position of maximum transverse electric field is a position of minimum transverse magnetic field.

III. CONSTRUCTION OF THE ANTENNA

In the order to construct an antenna to operate in the manner desired, i.e., with elliptical polarization and with a hemispherical radiation pattern, the following conditions must be fulfilled:

(A) The two orthogonal electric field components must be equal in magnitude.

(B) There must be a phase difference of $\pi/2$ between these components.

(C) There must be a perpendicular electric field component in the opening of each slot.

The electric field components are equal in magnitude if

$$K_x = K_y . \tag{72}$$

In the transverse electric mode solution (TE_{11}) this condition is obtained by constructing a cavity with equal dimensions (a = b). Thus the cavity should be square with a length equal to one-half the waveguide wave-length, $\frac{\lambda_g}{2}$. The cavity is magnetically coupled to the source by the use of two coupling loops. These loops are placed in the base of the cavity which is a region of maximum magnetic field intensity because the transverse electric field must be zero in this region if the boundary conditions are to be satisfied. The cavity may also be coupled through a probe inserted in an electric field maximum. The placement may be in the sidewalls, but this would preclude the use of the cavity element in an antenna array with close element spacing.

To introduce a time phase shift of $\pi/2$ between the electric field components, one of the loops is fed with a line which is $\lambda/4$ longer than the feed line to the other coupling loop. Therefore the following conditions are fulfilled: The two equal electric field components are orthogonal in space with a time phase difference of $\pi/2$.

The cavity may be represented by an equivalent circuit of lumped parameters. An equivalent circuit is given by Montgomery, Dicke and Purcell[7] for a loop-coupled cavity near resonance in Figure 9. The equivalent circuit has been modified to include a two loop input rather than a single loop and a representation to denote coupling out of the cavity through the radiating slots. The cavity is coupled to the feed lines through the loops represented by $L_{in}(1)$ and $L_{in}(1)$. The degree of coupling is denoted by a coupling coefficient, β. There is a mutual coupling coefficient, M, present between the feed loops. At resonance the cavity may be represented by a loss resistance and the reflected radiation resistance of the slot antenna R_a. This portion of the circuit may not be simplified because of the undertermined nature of the output coupling coefficients β_2 and β_2'. At resonance the slot antenna appears as pure resistance.

It is apparent β_1 and β_1' should be equal in magnitude and as close to unity as possible. This allows the maximum amount of energy to be coupled into the cavity. The standing wave ratio r, must be equal to unity to fulfill this condition. The standing

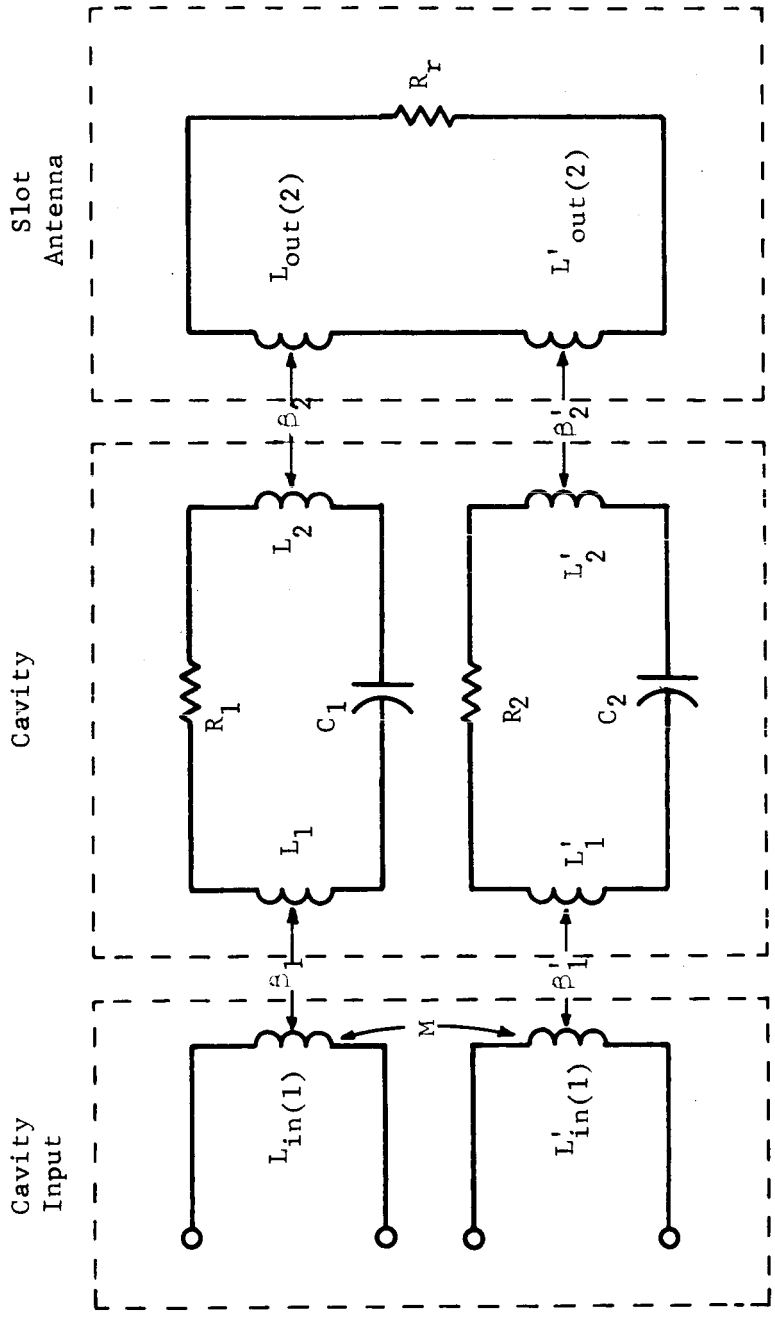

Fig. 9--The Equivalent Circuit for the Crossed-Slot, Cavity Backed Antenna

wave ratio is defined as

$$r = \frac{1 + |\Gamma|}{1 - |\Gamma|} , \tag{73}$$

where Γ is the reflection coefficient which gives the percent of energy reflected. For a coupling coefficient of unity, $\Gamma = 0$. A standing wave ratio of unity denotes a perfect match to the input feed structure and the feed will undergo no impedance changes if the length of the feed line is changed.

The physical size of the cavity may be reduced by the insertion into the cavity of a dielectric with a relative permittivity greater than unity. This changes the velocity of propagation by a factor

$$V_{(\text{dielectric})} = \frac{V_{(\text{free space})}}{\epsilon_r} \tag{74}$$

which in turn decreases the wavelength.

Table (1) gives values for cavity dimensions at the desired frequency of operation.

Figure (10) shows a photograph of the crossed-slot antenna.

Figure (11) shows a comparison photograph of the unloaded and dielectric loaded antenna cavities.

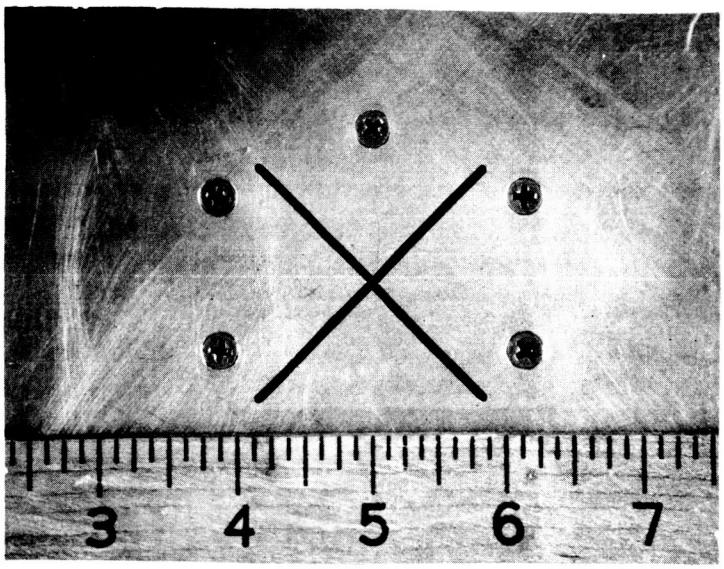

Fig. 10--A Photograph of the Crossed-Slot Antenna

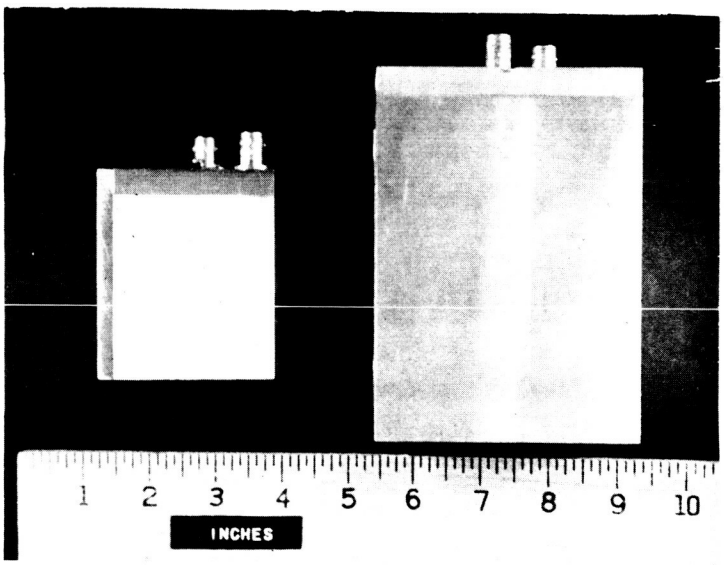

Fig. 11--A Photograph of the Rexolite Dielectric Loaded Cavity on the Left and the Unloaded Antenna Cavity on the Right

TABLE 1

COMPARISON OF THE AIR DIELECTRIC ANTENNA CAVITY AND REXOLITE DIELECTRIC LOADED ANTENNA CAVITY

Material	Aluminum	Aluminum
Dielectric	Air	Rexolite
Relative Permittivity	1	2.54
Cut-Off Frequency (f_c)	1.90 kmc	1.90 kmc
Operating Frequency (f_o) ($f_o = 1.2f_c$)	2.28 kmc	2.28 kmc
Width (a = b)	7.9 cm	4.9 cm
Length $\frac{\lambda_g}{2}$	11.9 cm	7.35 cm
Feed Type	Fixed Loops	Loops with series capacitor
Input Impedance	50 ohms	50 ohms
Voltate Standing Wave Ratio (VSWR)	1.1	1.05
Tuning	Adjustable slug in bottom face	Adjustable slug in bottom face

IV. EXPERIMENTAL EVALUATION

The test antennas constructed were tested on an outdoor antenna range. The antenna without dielectric loading exhibited a maximum variation in polarization of 3 db. in the forward direction. The variation in gain for various polarizations became greater for increasing angle away from the normal to the plane of the antenna. The polarization pattern did not exhibit any nulls over a large variation in angle from the normal.

The antenna beamwidth, or the angle at which the power drops to 3 db. of its maximum is approximately seventy degrees (70^{o}). The gain showed a variation of only 10 db. over a 132^{o} beamwidth. These patterns were obtained with a ground-plane of less than $10\lambda \times 10\lambda$. The beamwidth should be much improved by the use of a much larger ground plane.

The dielectric loaded antenna exhibited a maximum variation in polarization of approximately 4 db. in the forward direction. The polarization deteriorated for larger deviation in angle from the normal to the antenna surface but no nulls were recorded over a very large beamwidth of the antenna.

The dielectric loaded antenna beamwidth (3 db.) is approximately 95^{o} for an elevation cut along one of the slot antennas and approximately 65^{o} in the plane of maximum variation ($\phi = 45^{o}$). This beamwidth is

satisfactory since the beam may be widened through the utilization of a much larger ground plane.

The graphs in Appendix A and Appendix B were plotted on a Scientific-Atlanta automatic pattern recorder. This device automatically plots the power received by the test antenna as a function of antenna position as the antenna position is varied.

V. CONCLUSIONS

The test antennas exhibited the desired properties of elliptical polarization and a large, if not hemispherical, beamwidth. As was previously mentioned the beamwidth is dependent on the ground plane configuration and therefore the slot antenna should be used with a large metallic sheet to obtain the desired hemispherical radiation characteristic.

The antenna appears to be applicable to electronic scanning techniques when used as an element in an array. The actual change necessary to scan the array can be made prior to the application of the signal to the array element.

REFERENCES

1. A. Z. Fradin, Microwave Antennas, trans. Morton Nadler (London: Pergamon Press, 1961), p. 456, p. 463.

2. John M. Stone, Radiation and Optics, (New York: McGraw-Hill Book Company, 1963), p. 167.

3. Henry Jasik (Ed.), Antenna Engineering Handbook, (New York: McGraw-Hill Book Company, 1961) pp. 8-5.

4. John D. Kraus, Antennas, (New York: McGraw-Hill Book Company, 1950), pp. 464-467.

5. Lewis C. Martin, "An Analytical Evaluation of the Mills Cross and the Two-Dimensional Matrix Antenna Array", (unpublished Masters' thesis, Department of Electrical Engineering, Auburn University, 1964), p. 12.

6. Simon Ramo and John R. Whinnery, Fields and Waves in Modern Radio, (New York: John Wiley and Sons, 1953), pp. 283-284, pp. 355-356.

7. C. G. Montgomery, R. H. Dicke, and E. M. Purcell, Principles of Microwave Circuits , Vol. VIII of the M.I.T. Radiation Laboratory Series, ed. Louis N. Ridenous (28 vols.; Lexington, Massachusetts: Boston Technical Publishers, 1964), p. 227.

APPENDIX A

The Aximuth and Elevation Field Patterns of the Air Dielectric, Crossed-Slot Antenna are as Follows:

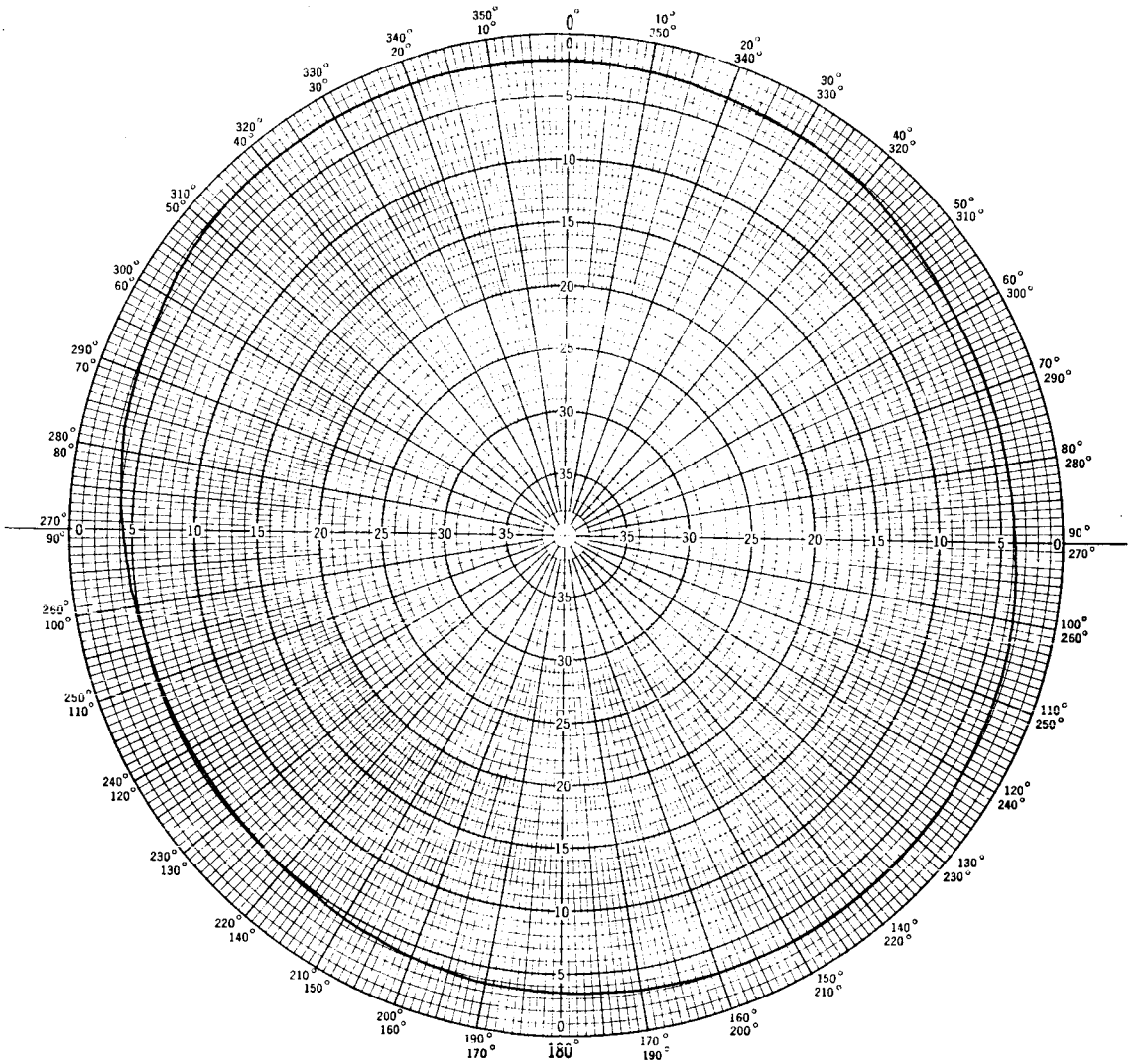

Fig. A-1--The Azimuth Pattern of the Air Dielectric Crossed-Slot Antenna ($\theta = 0^{\circ}$)

Polar Chart No. 127D
SCIENTIFIC-ATLANTA, INC.
ATLANTA, GEORGIA

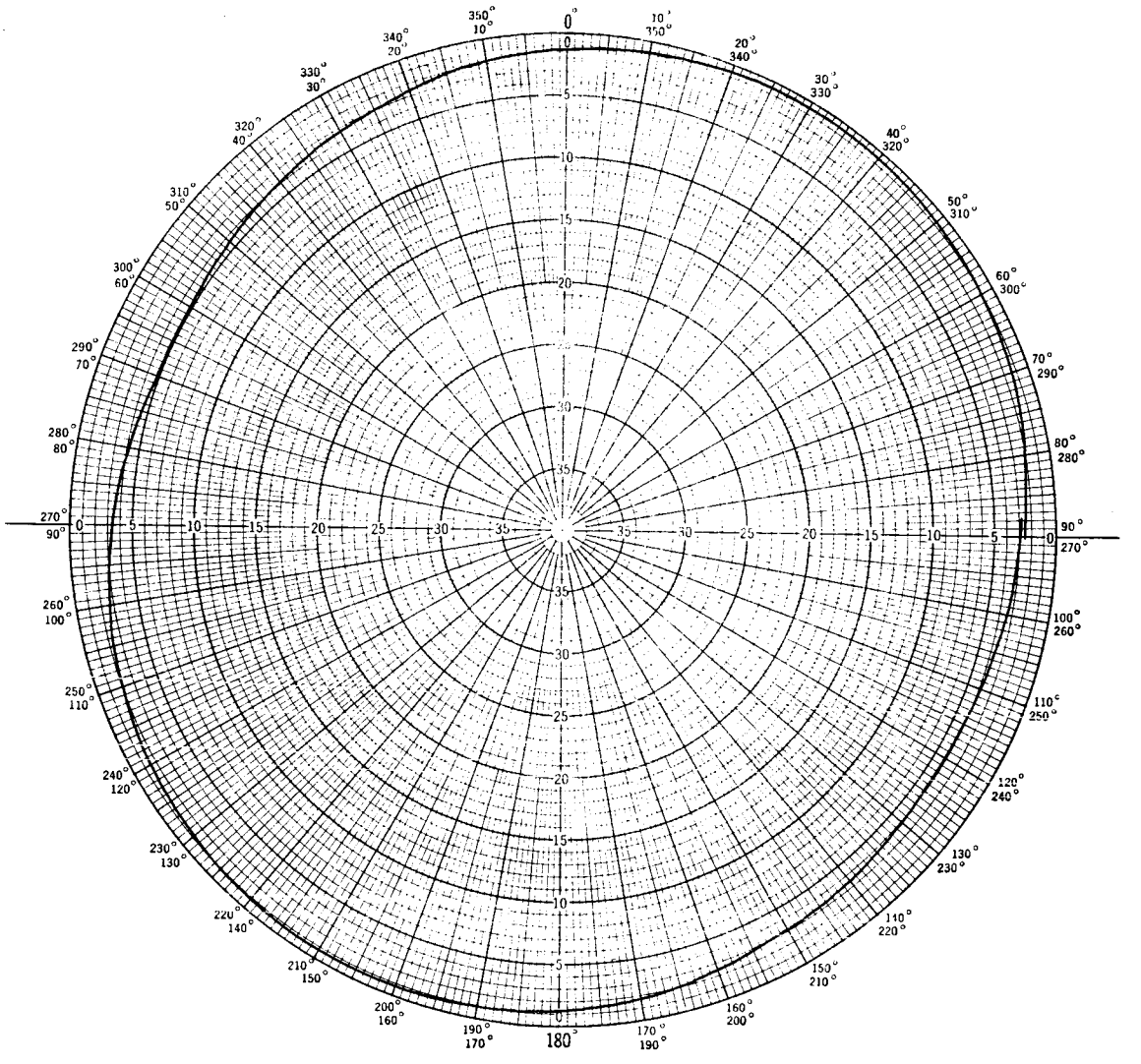

Fig. A-2--The Azimuth Pattern of the Air Dielectric Crossed-Slot Antenna ($\theta = 5^{o}$)

Polar Chart No. 127D
SCIENTIFIC-ATLANTA, INC.
ATLANTA, GEORGIA

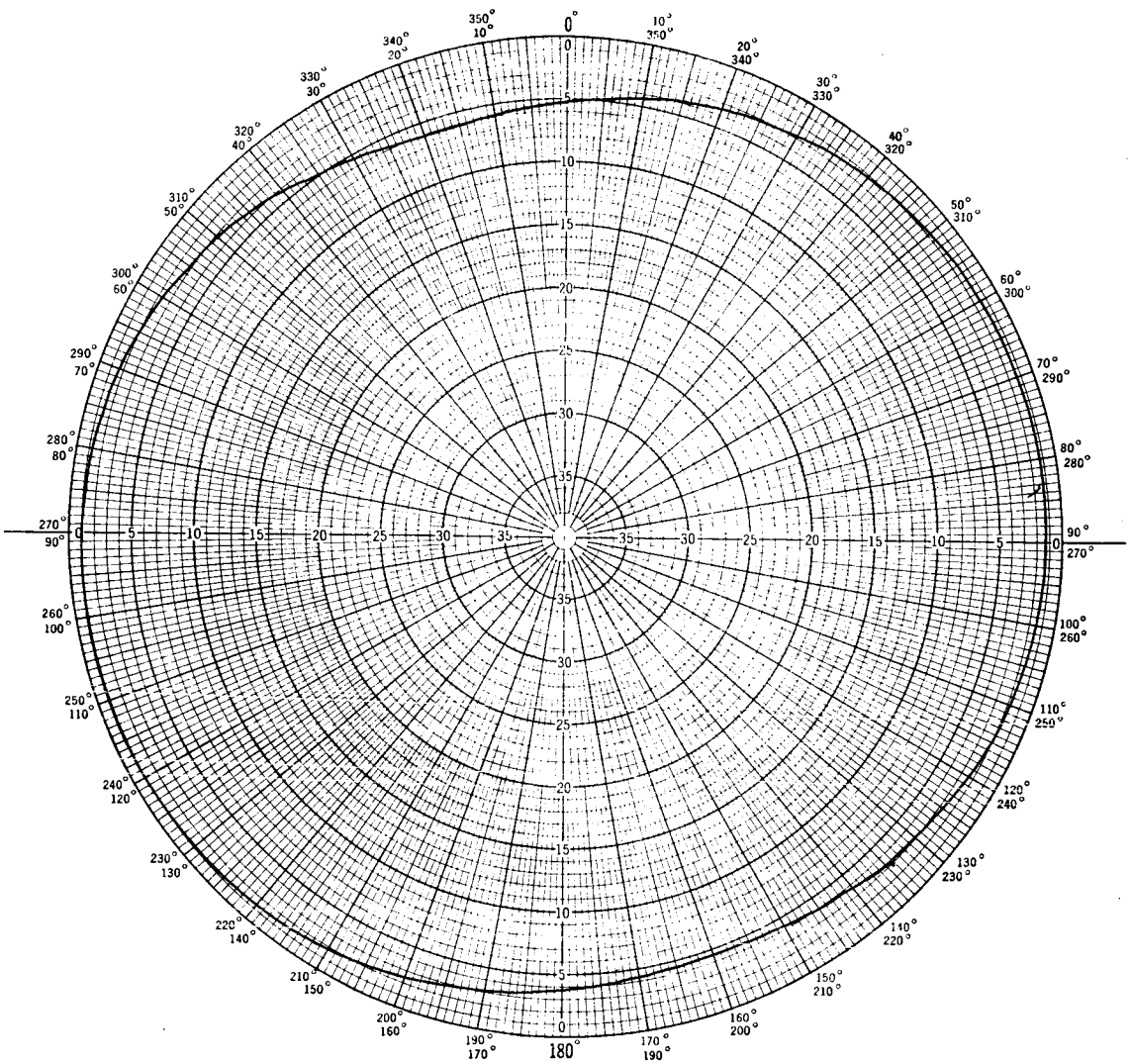

Fig. A-3--The Azimuth Pattern of the Air Dielectric Crossed-Slot Antenna ($\theta = 10^{\circ}$)

Polar Chart No. 127D
SCIENTIFIC-ATLANTA, INC.
ATLANTA, GEORGIA

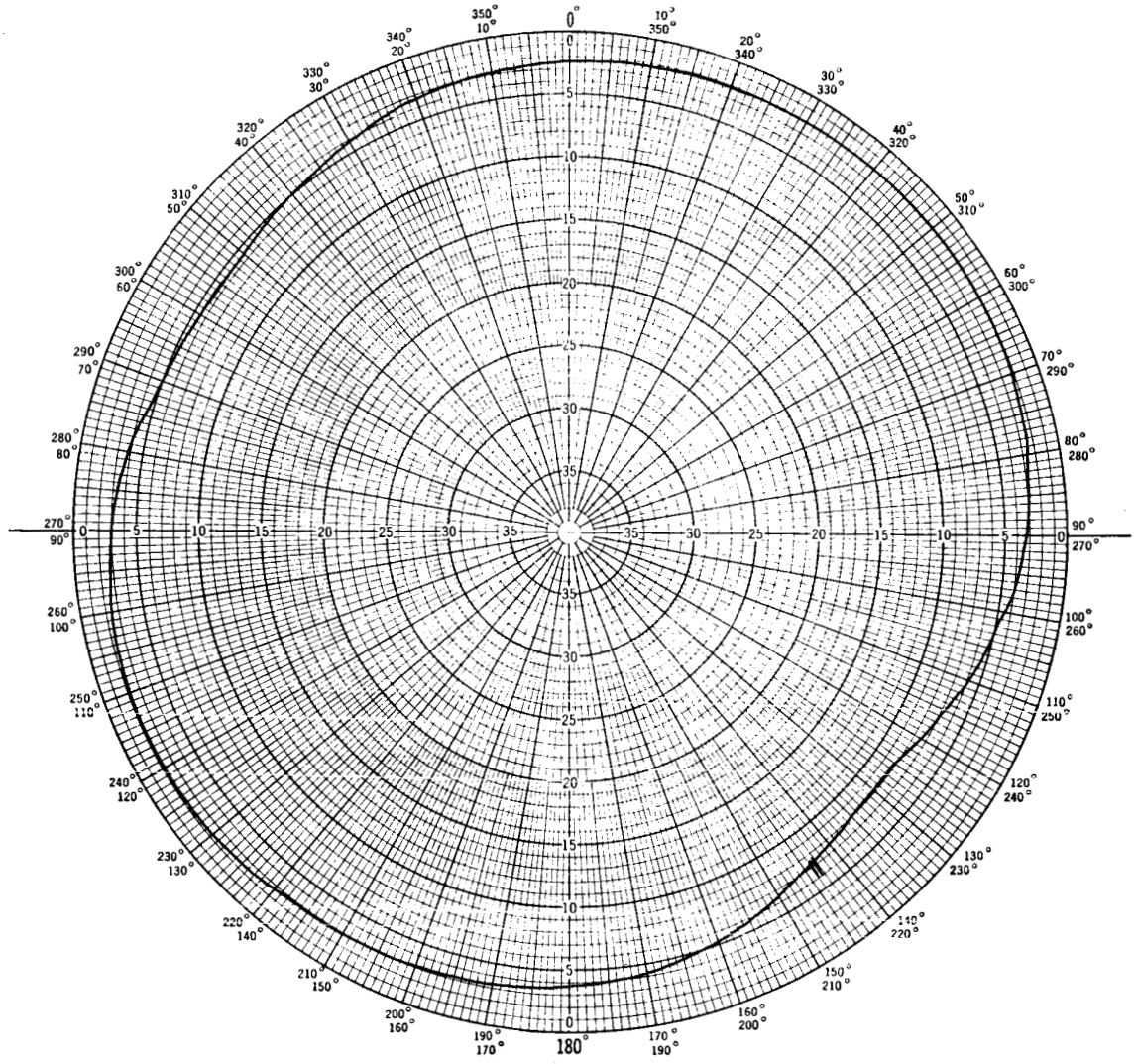

Fig. A-4--The Azimuth Pattern of the Air Dielectric Crossed-Slot Antenna ($\theta = 15^{\circ}$)

Polar Chart No. 127D
SCIENTIFIC-ATLANTA, INC.
ATLANTA, GEORGIA

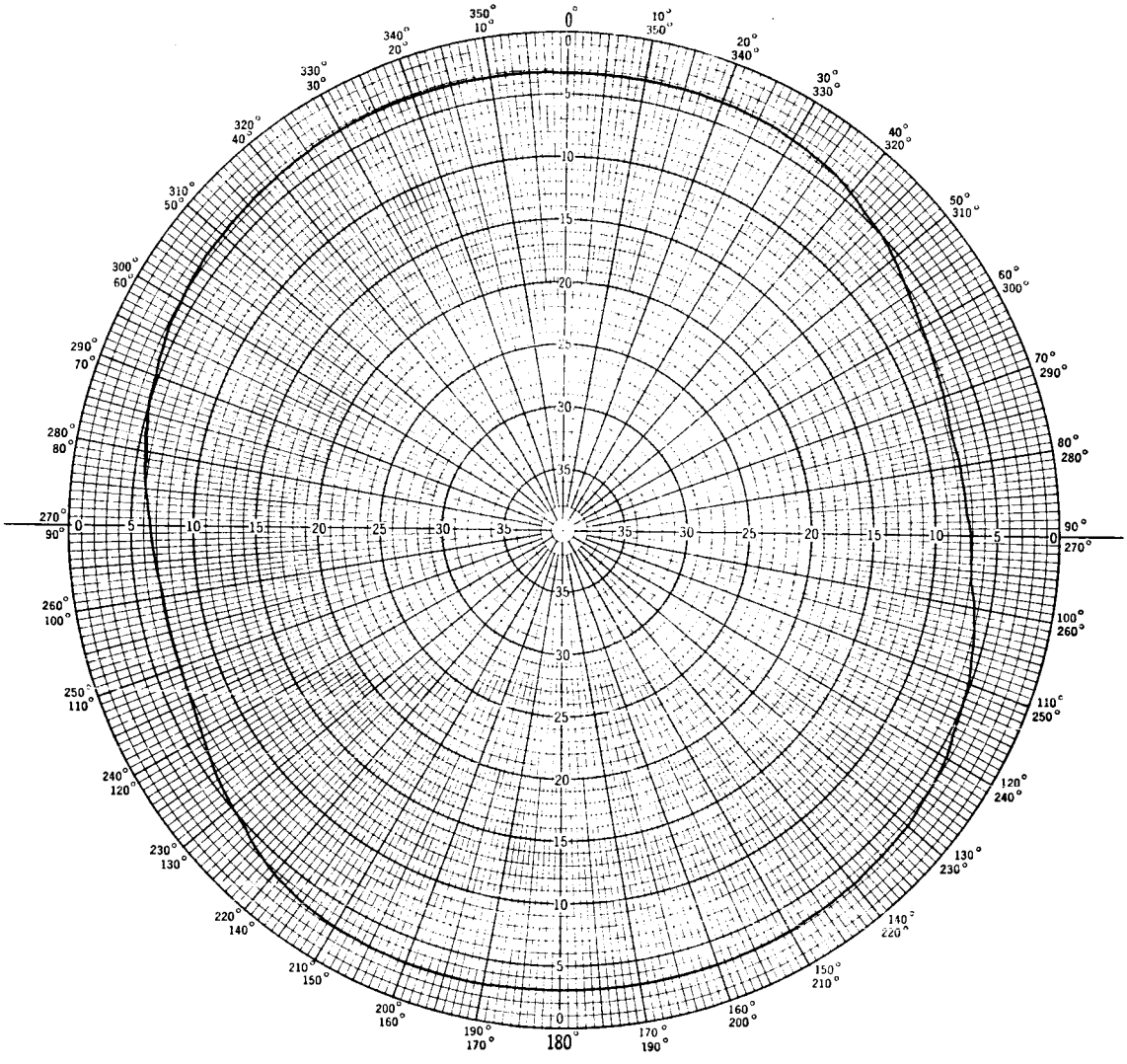

Fig. A-5--The Azimuth Pattern of the Air Dielectric Crossed-Slot Antenna (θ - 20°)

Polar Chart No. 127D
SCIENTIFIC-ATLANTA, INC.
ATLANTA, GEORGIA

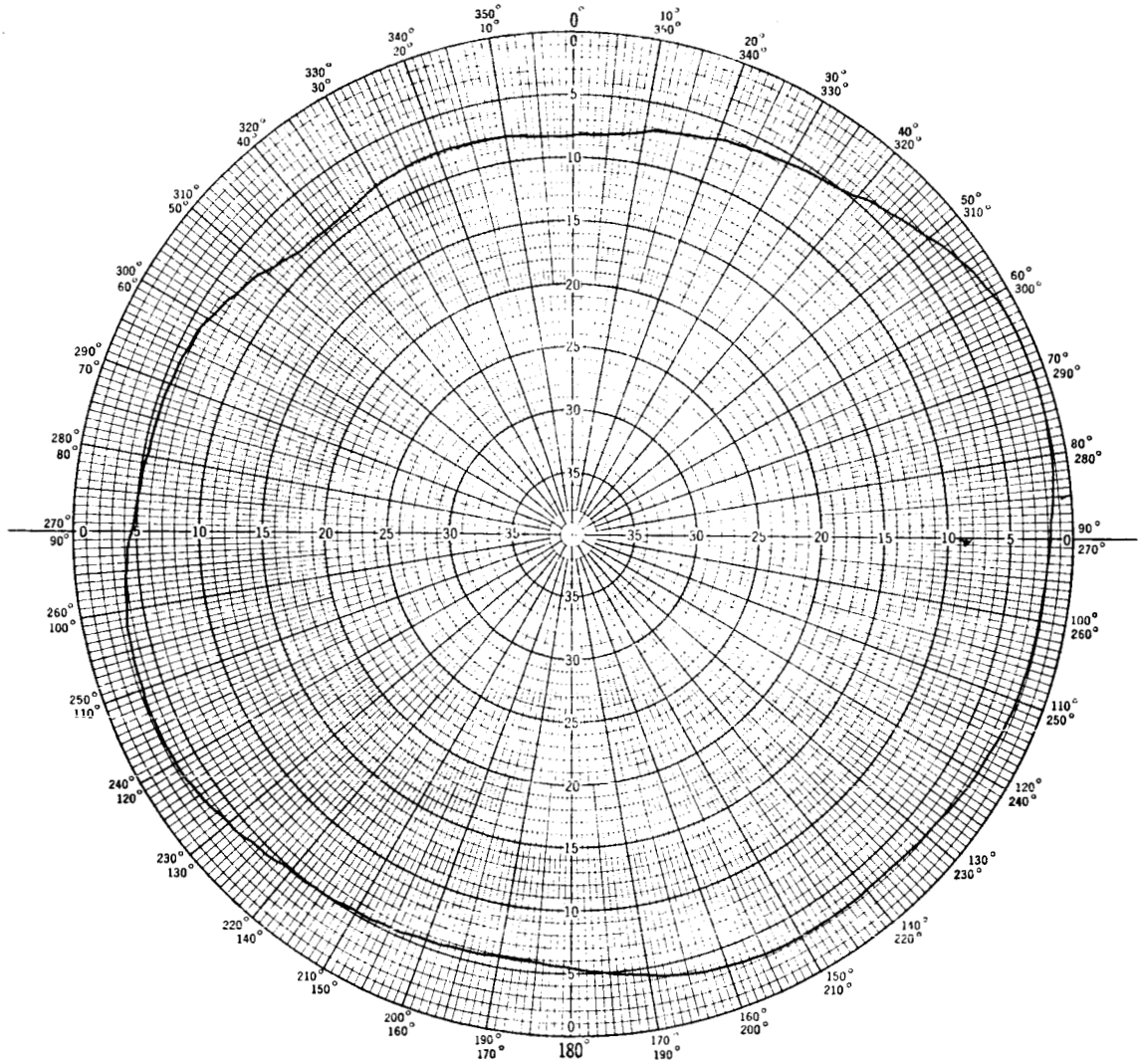

Fig. A-6--The Azimuth Pattern of the Air Dielectric Crossed-Slot Antenna ($\theta = 30^{\circ}$)

Polar Chart No. 127D
SCIENTIFIC-ATLANTA, INC.
ATLANTA, GEORGIA

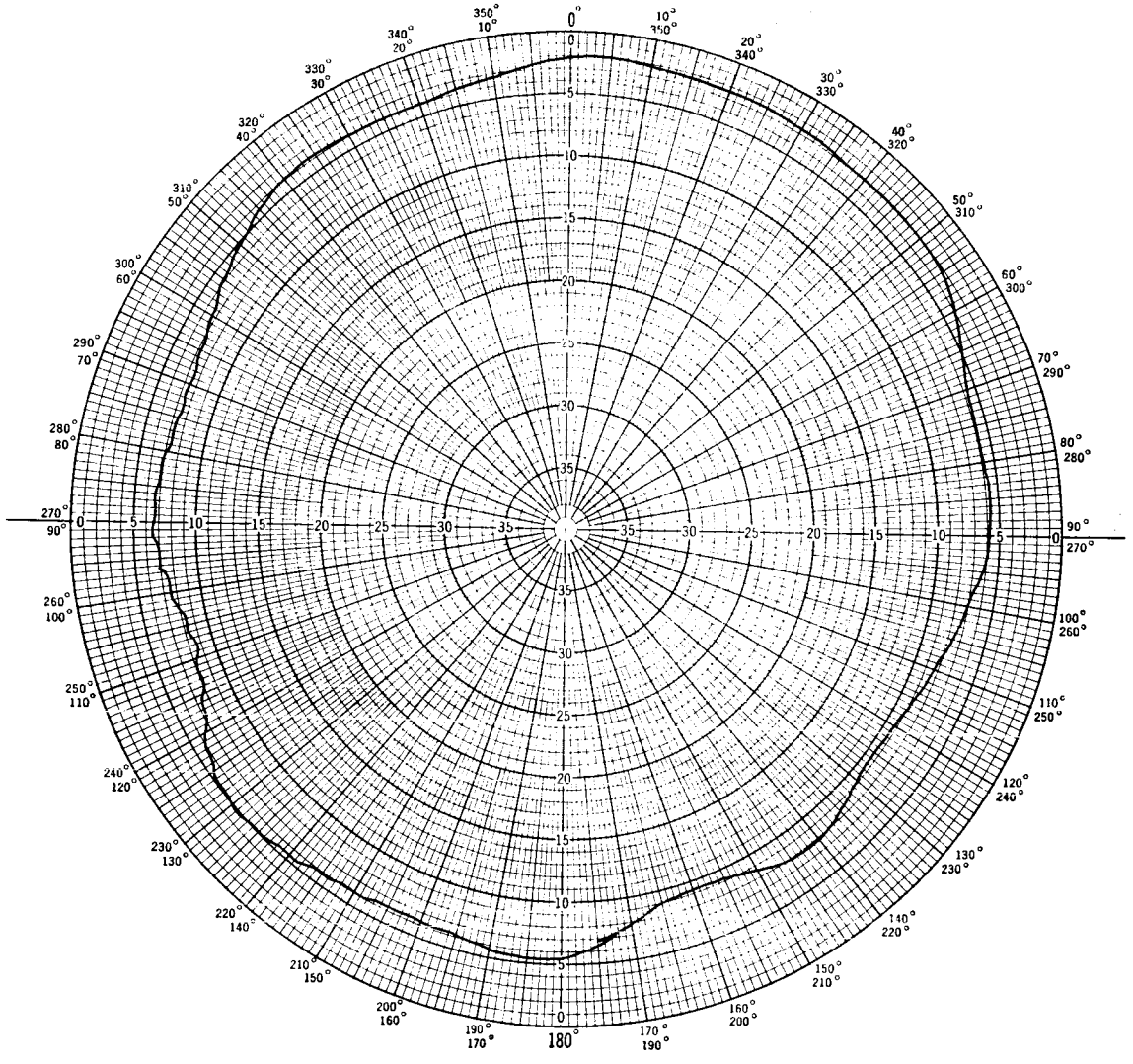

Fig. A-7--The Azimuth Pattern of the Air Dielectric Crossed-Slot Antenna ($\theta = 40°$)

Polar Chart No. 127D
SCIENTIFIC-ATLANTA, INC.
ATLANTA, GEORGIA

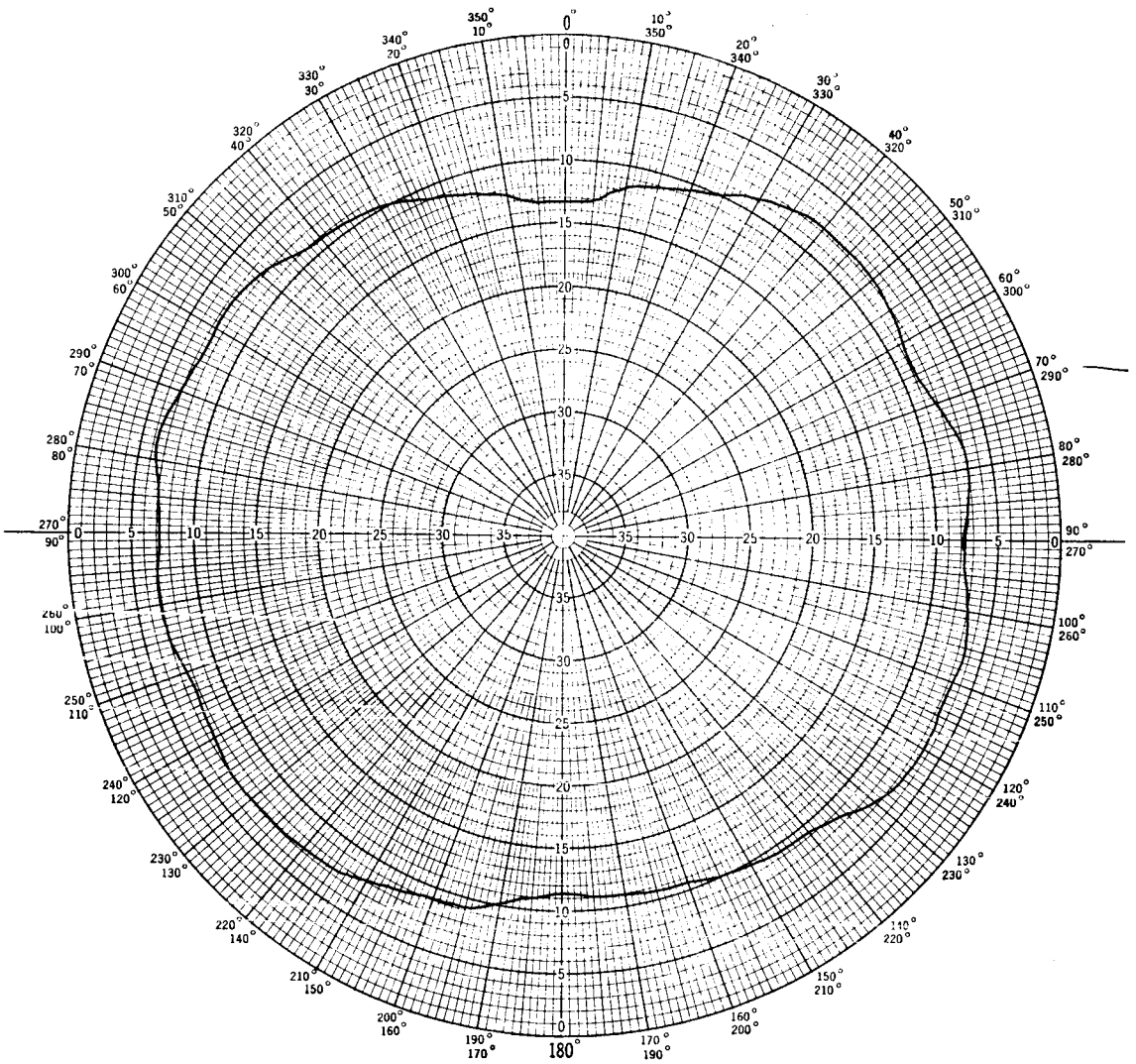

Fig. A-8--The Azimuth Pattern of the Air Dielectric Crossed-Slot Antenna ($\theta = 50^{o}$)

Polar Chart No. 127D
SCIENTIFIC-ATLANTA, INC.
ATLANTA, GEORGIA

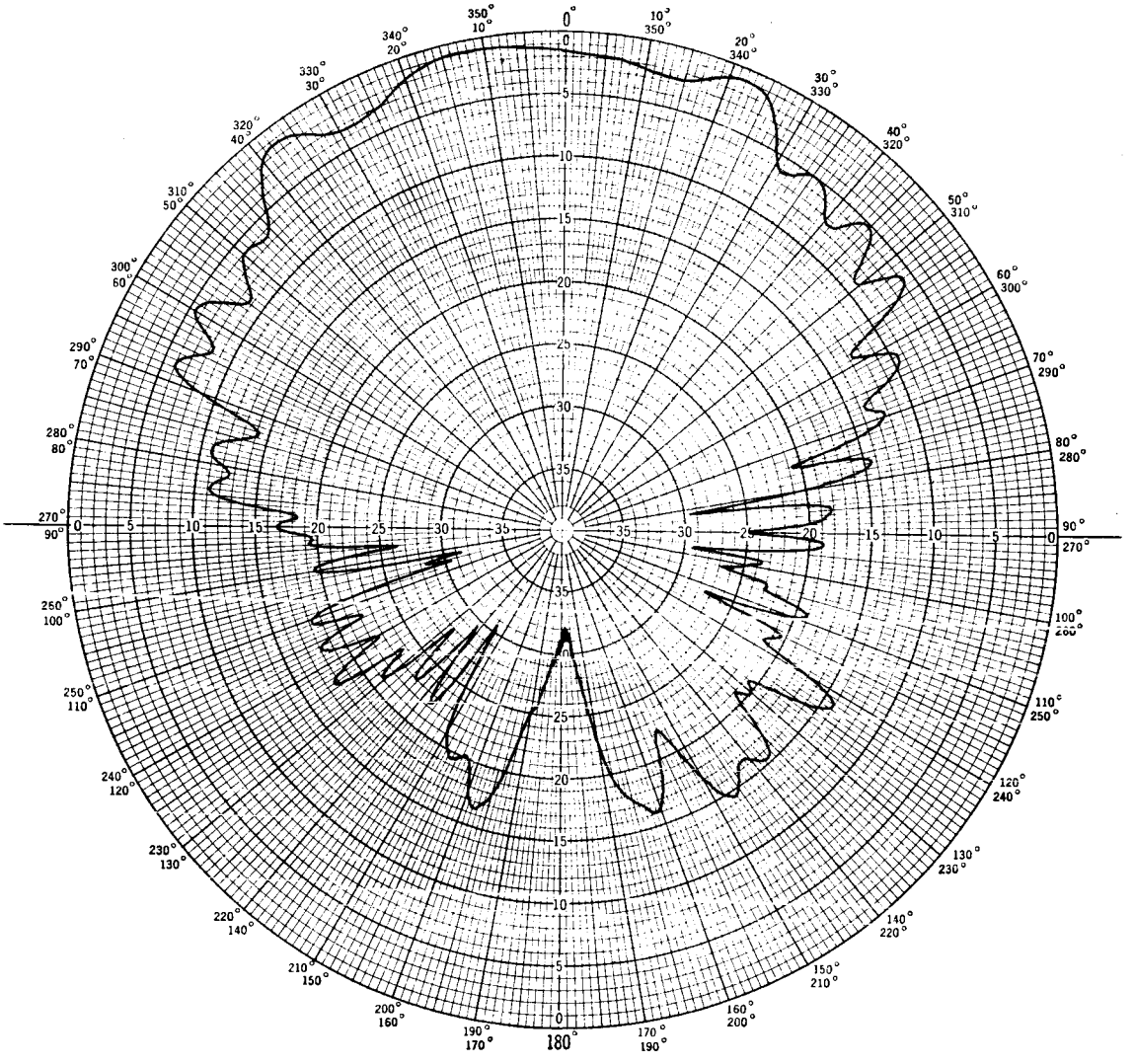

Fig. A-9--The Elevation Pattern of the Air Dielectric Crossed-Slot Antenna

Polar Chart No. 127D
SCIENTIFIC-ATLANTA, INC.
ATLANTA, GEORGIA

APPENDIX B

The Azimuth and Elevation Field Patterns of the Rexolite Dielectric Loaded Crossed-Slot Antenna are as Follows:

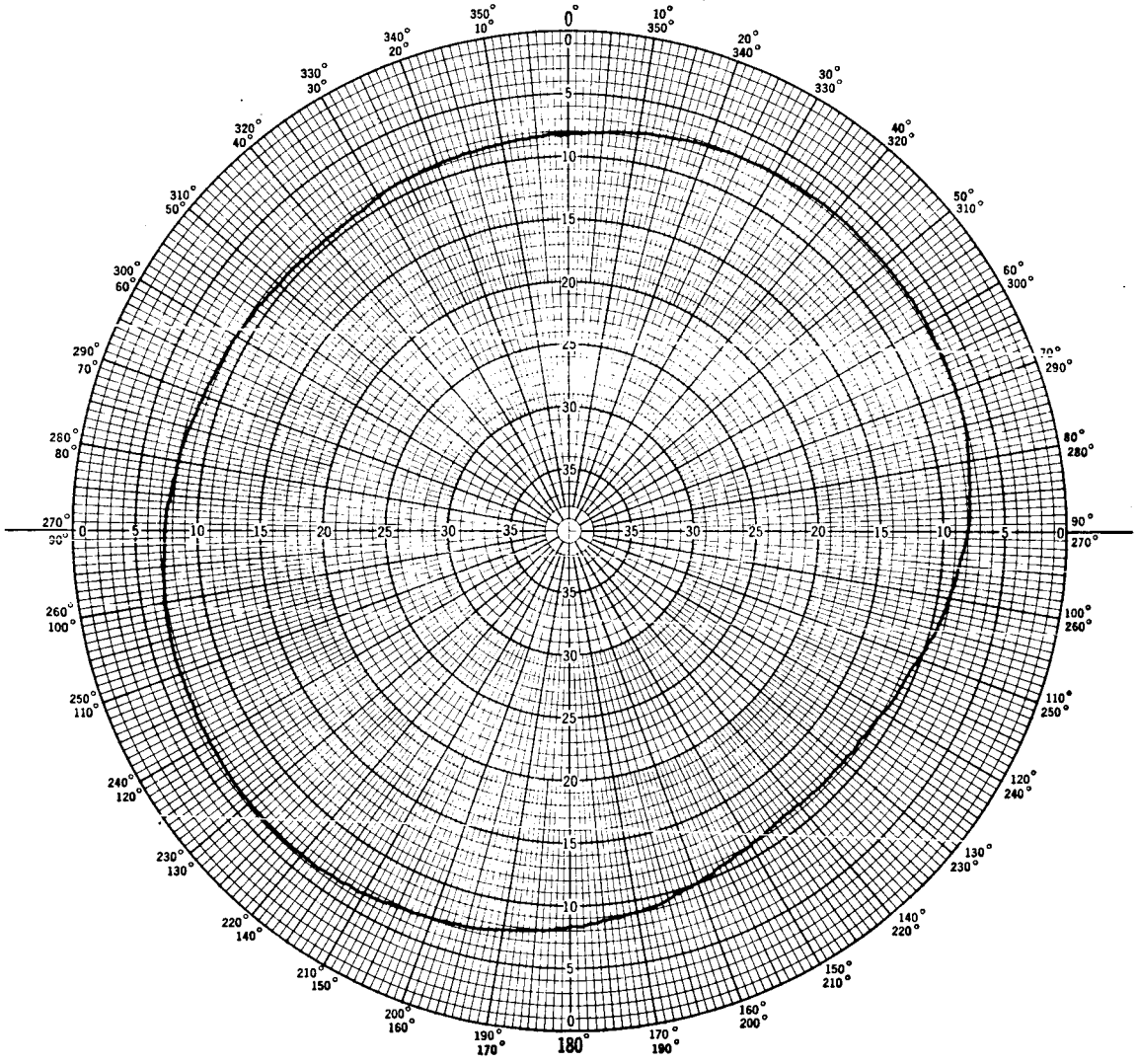

Fig. B--The Azimuth Pattern of the Rexolite Dielectric Loaded Crossed-Slot Antenna ($\theta = 0$)

Polar Chart No. 127D
SCIENTIFIC-ATLANTA, INC.
ATLANTA, GEORGIA

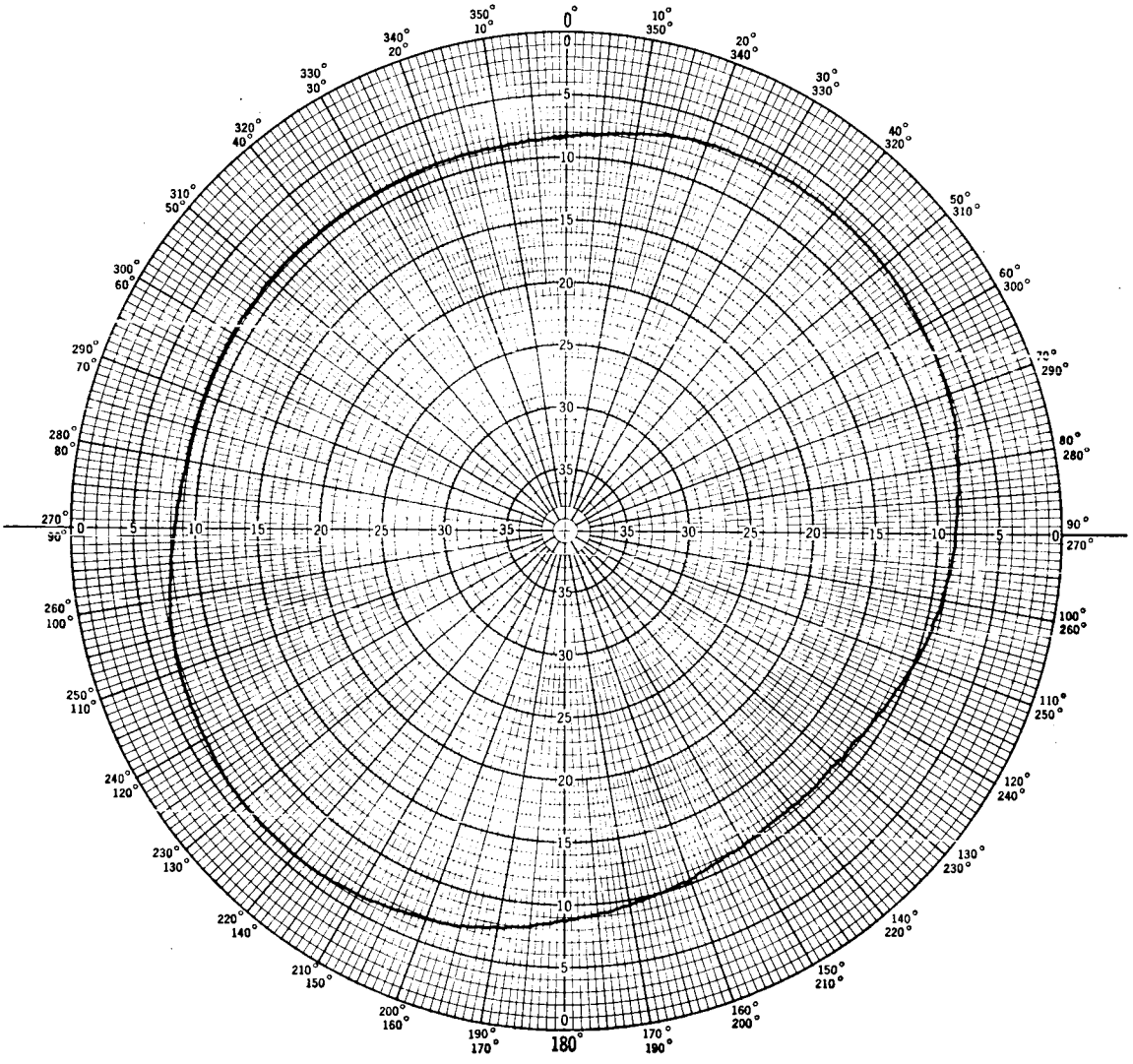

Fig. B-2--The Azimuth Pattern of the Rexolite Dielectric Loaded Crossed-Slot Antenna ($\Theta = 5^{O}$)

Polar Chart No. 127D
SCIENTIFIC-ATLANTA, INC.
ATLANTA, GEORGIA

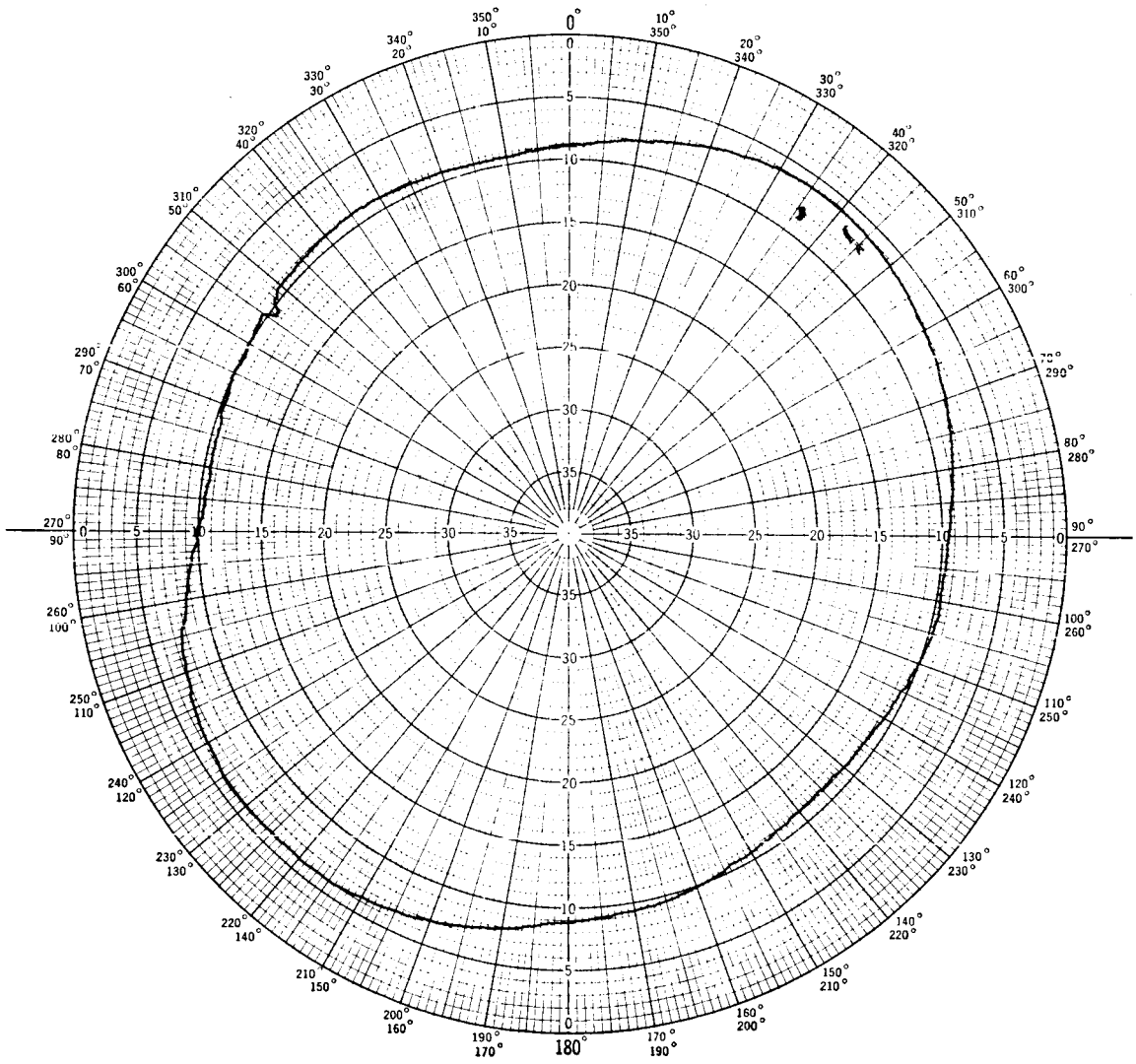

Fig. B-3--The Azimuth Pattern of the Rexolite Dielectric Loaded Crossed-Slot Antenna ($\theta = 10^{o}$)

Polar Chart No. 127D
SCIENTIFIC-ATLANTA, INC.
ATLANTA, GEORGIA

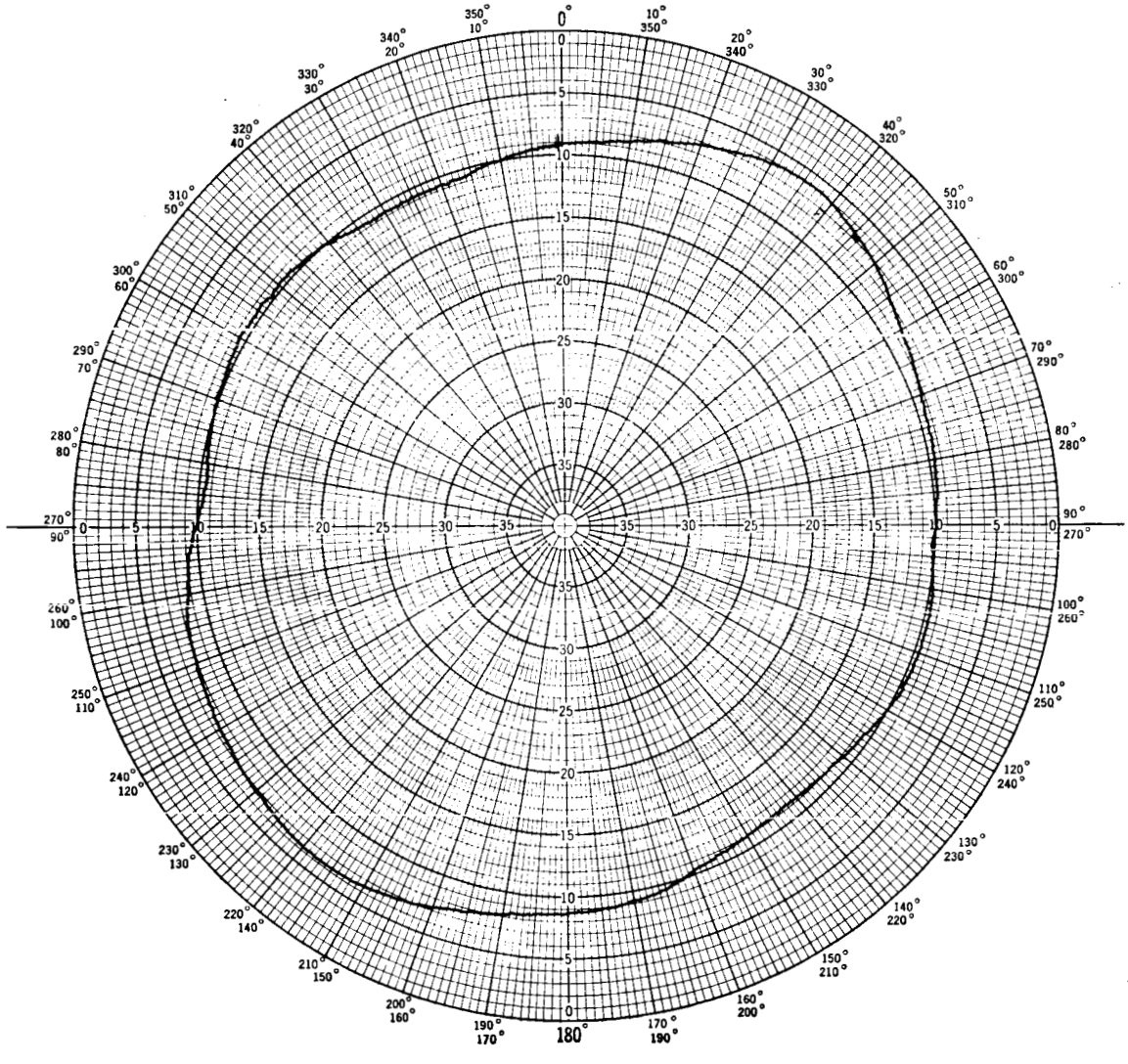

Fig. B-4--The Azimuth Pattern of the Rexolite Dielectric Loaded Crossed-Slot Antenna ($\theta = 15^{\circ}$)

Polar Chart No. 127D
SCIENTIFIC-ATLANTA, INC.
ATLANTA, GEORGIA

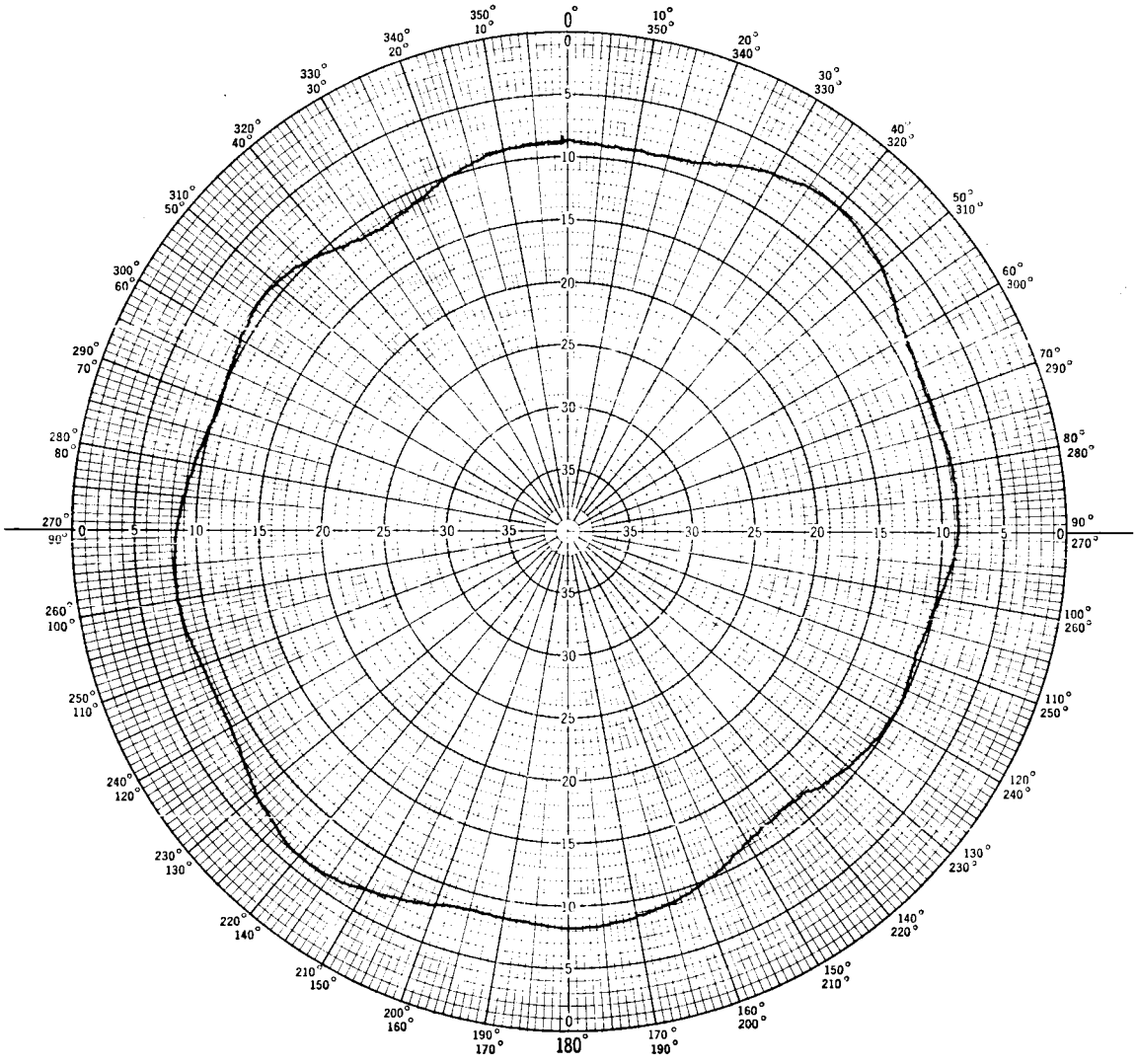

Fig. B-5--The Azimuth Pattern of the Rexolite Dielectric Loaded Crossed-Slot Antenna ($\theta = 20^{o}$)

Polar Chart No. 127D
SCIENTIFIC-ATLANTA, INC.
ATLANTA, GEORGIA

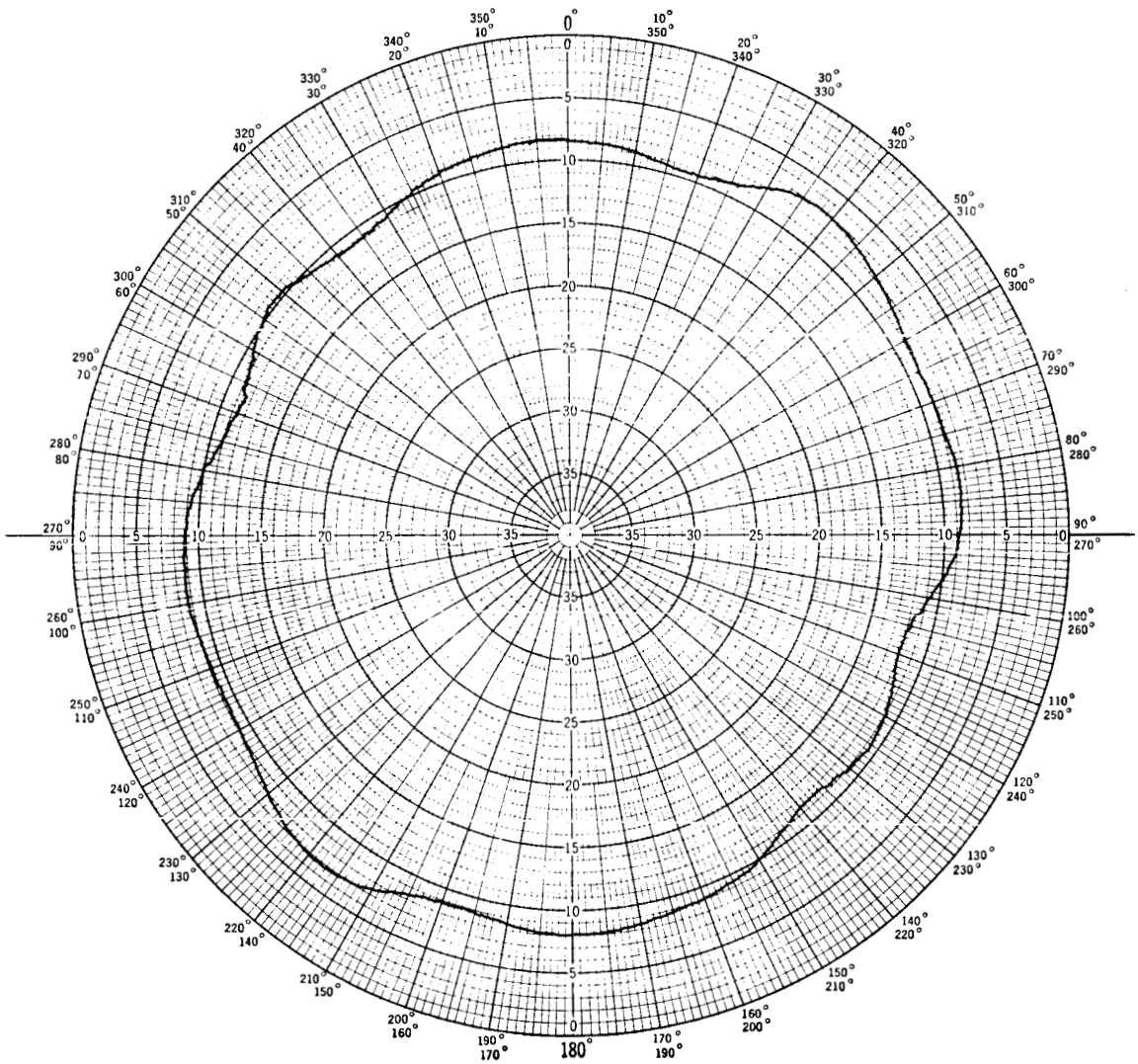

Fig. B-6--The Azimuth Pattern of the Rexolite Dielectric Loaded Crossed-Slot Antenna ($\theta = 25^{\circ}$)

Polar Chart No. 127D
SCIENTIFIC-ATLANTA, INC.
ATLANTA, GEORGIA

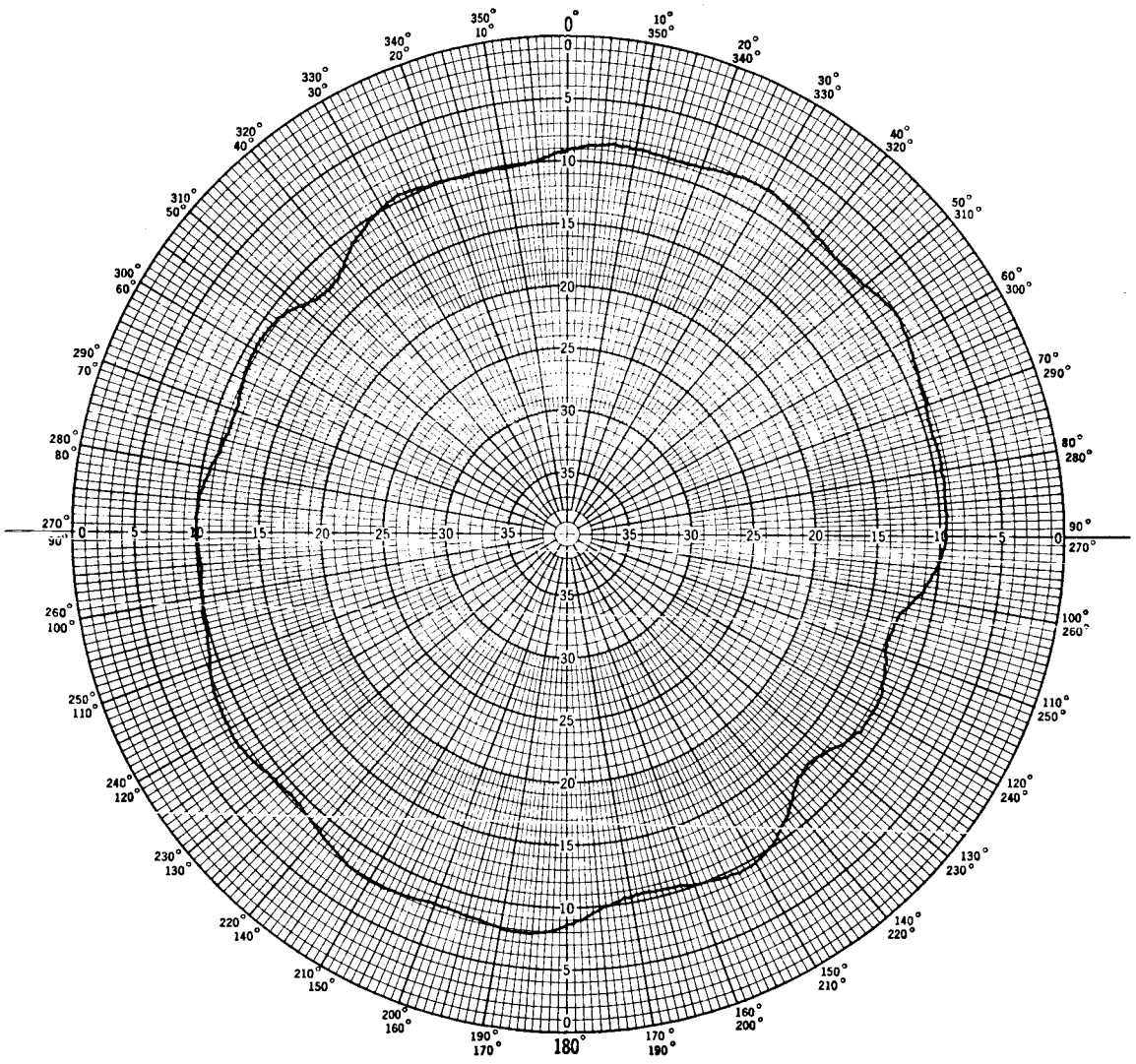

Fig. B-7--The Azimuth Pattern of the Rexolite Dielectric Loaded Crossed-Slot Antenna ($\theta = 30^{\circ}$)

Polar Chart No. 127D
SCIENTIFIC-ATLANTA, INC.
ATLANTA, GEORGIA

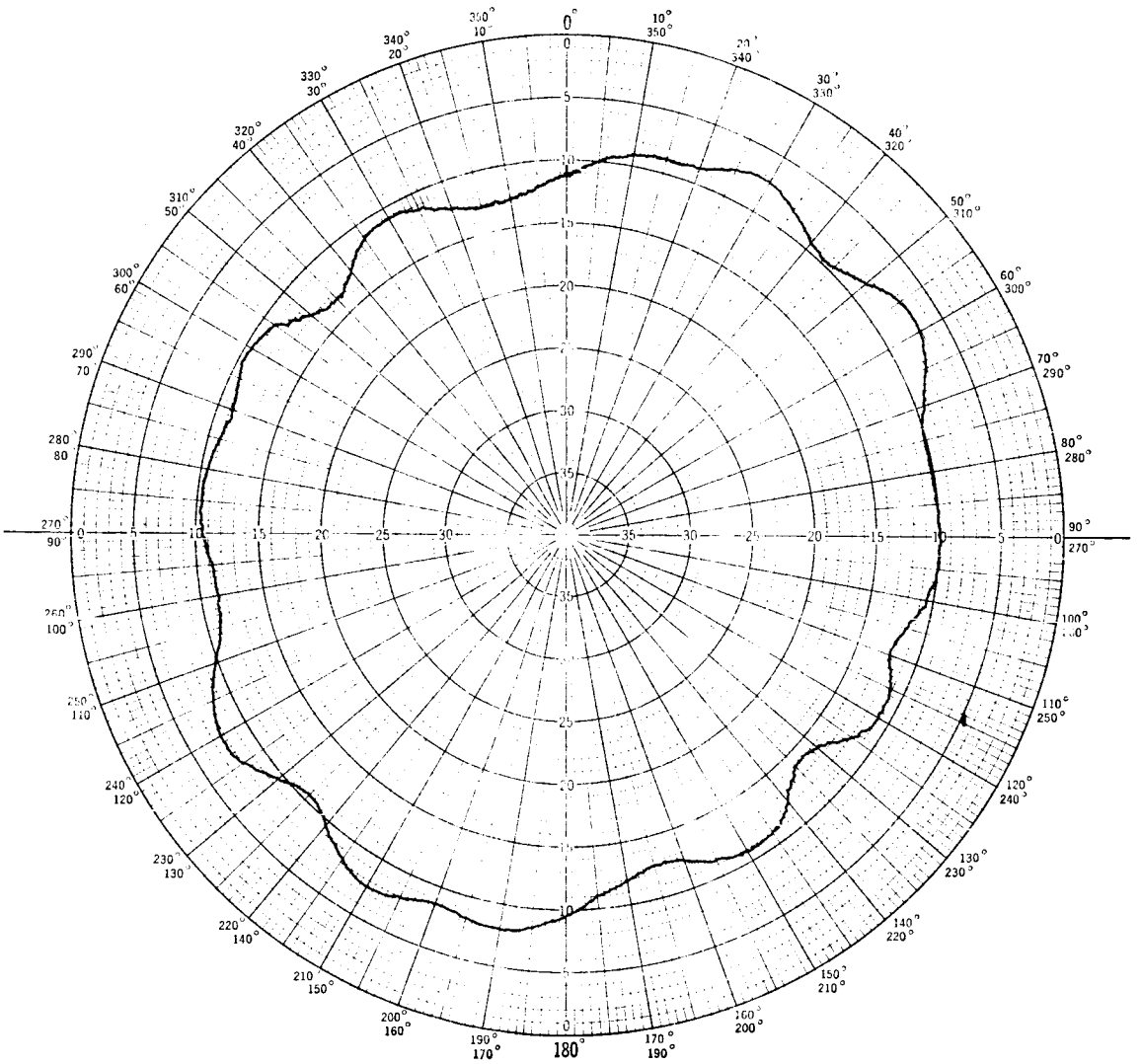

Fig. B-8--The Azimuth Pattern of the Rexolite Dielectric Loaded Crossed-Slot Antenna ($\theta = 35^{\circ}$)

Polar Chart No. 127D
SCIENTIFIC-ATLANTA, INC.
ATLANTA, GEORGIA

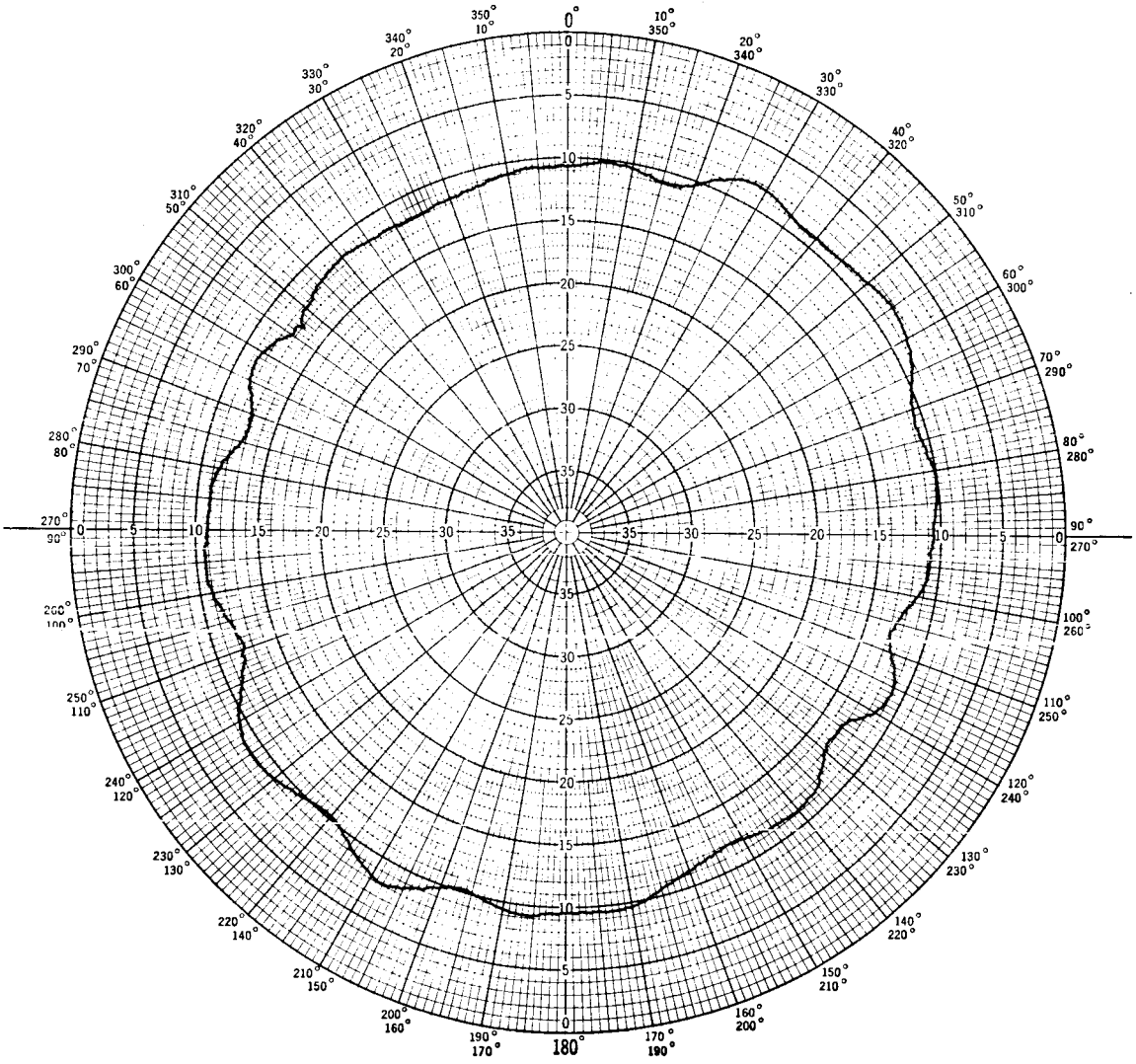

Fig. B-9--The Azimuth Pattern of the Rexolite Dielectric Loaded Crossed-Slot Antenna ($\Theta = 40^{o}$)

Polar Chart No. 127D
SCIENTIFIC-ATLANTA, INC.
ATLANTA, GEORGIA

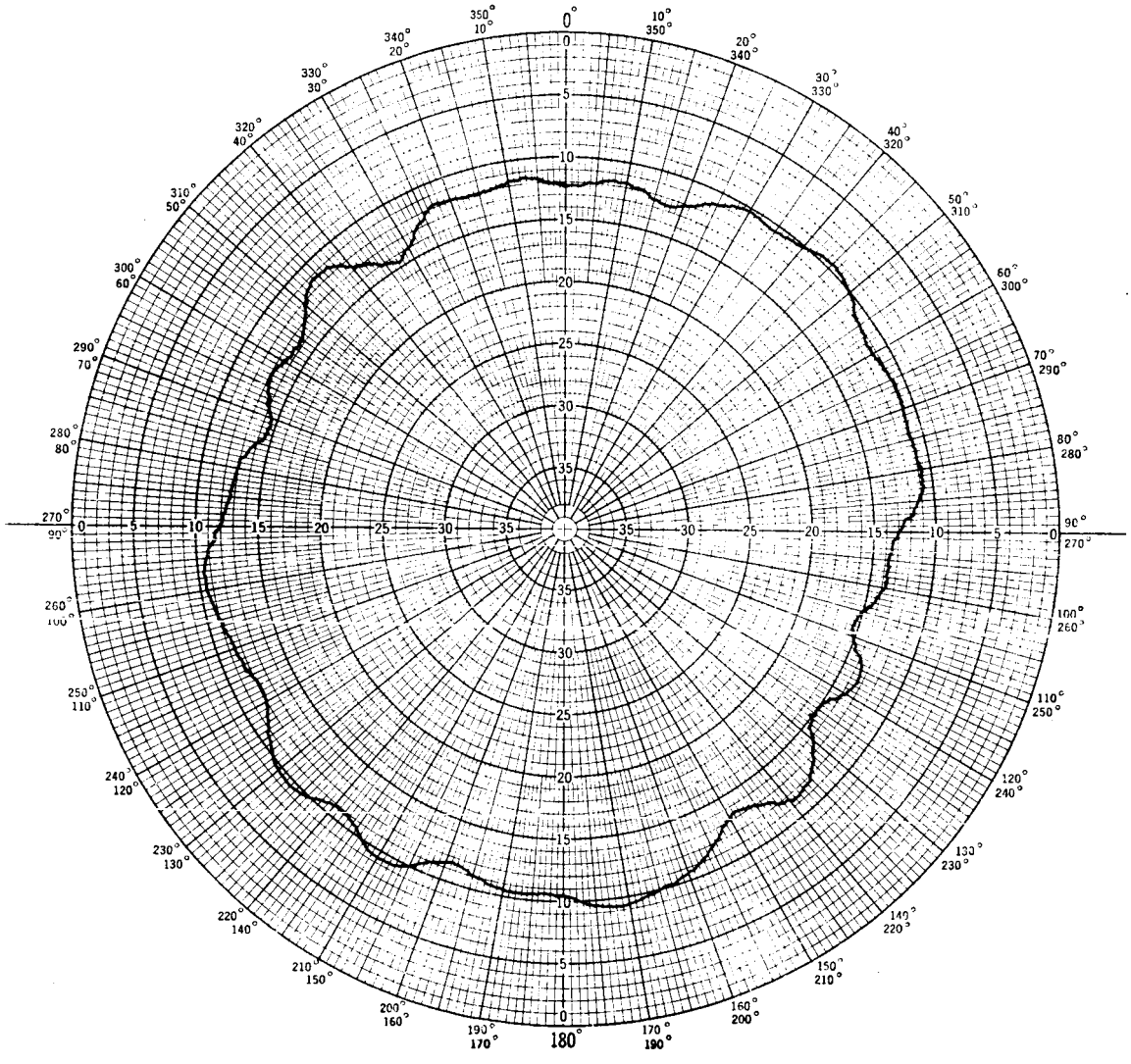

Fig. B-10--The Azimuth Pattern of the Rexolite Dielectric Loaded Crossed-Slot Antenna ($\theta = 45^{\circ}$)

Polar Chart No. 127D
SCIENTIFIC-ATLANTA, INC.
ATLANTA, GEORGIA

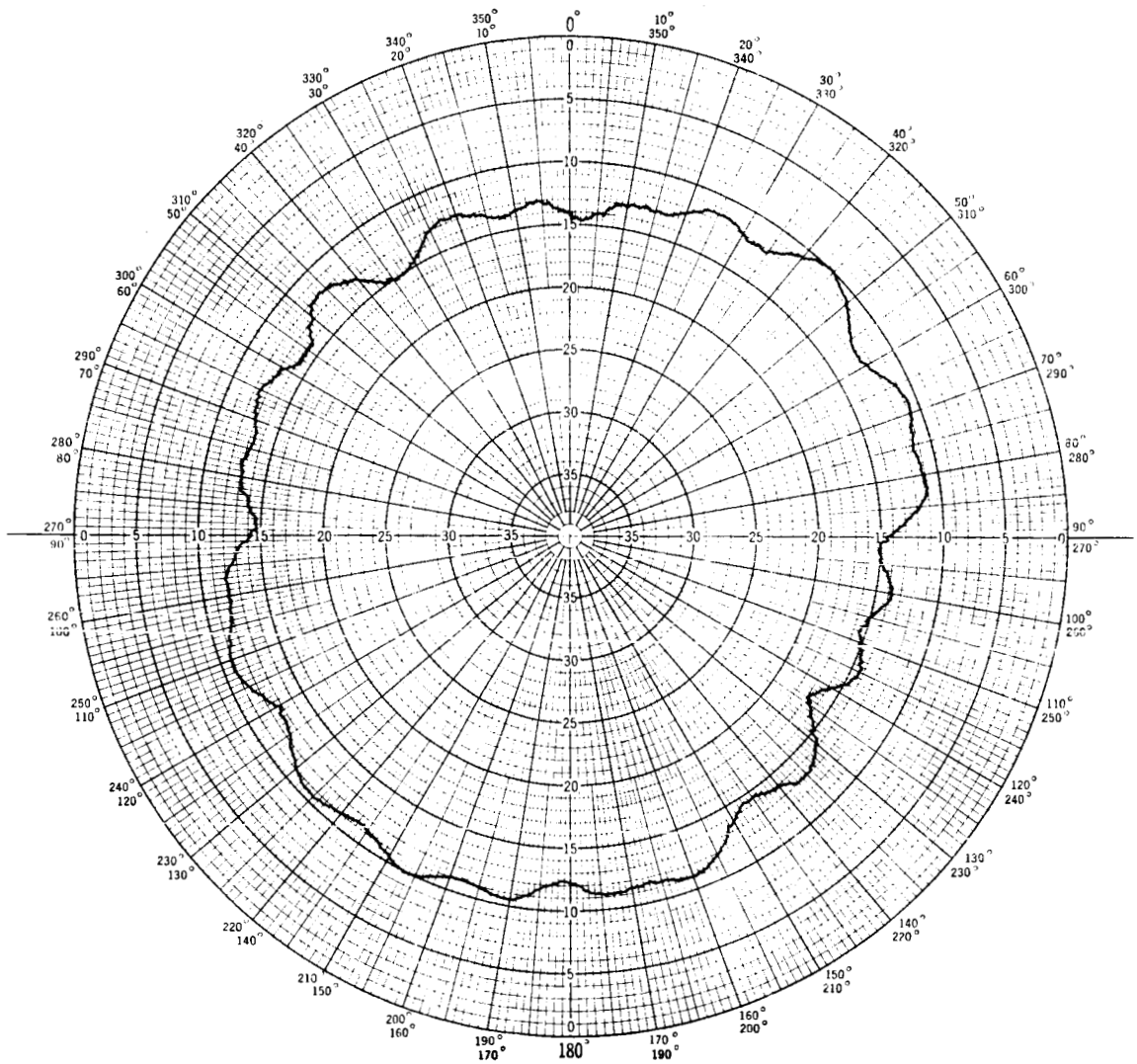

Fig. B-11--The Azimuth Pattern of the Rexolite Dielectric Loaded Crossed-Slot Antenna (θ = 50º)

Polar Chart No. 127D
SCIENTIFIC-ATLANTA, INC.
ATLANTA, GEORGIA

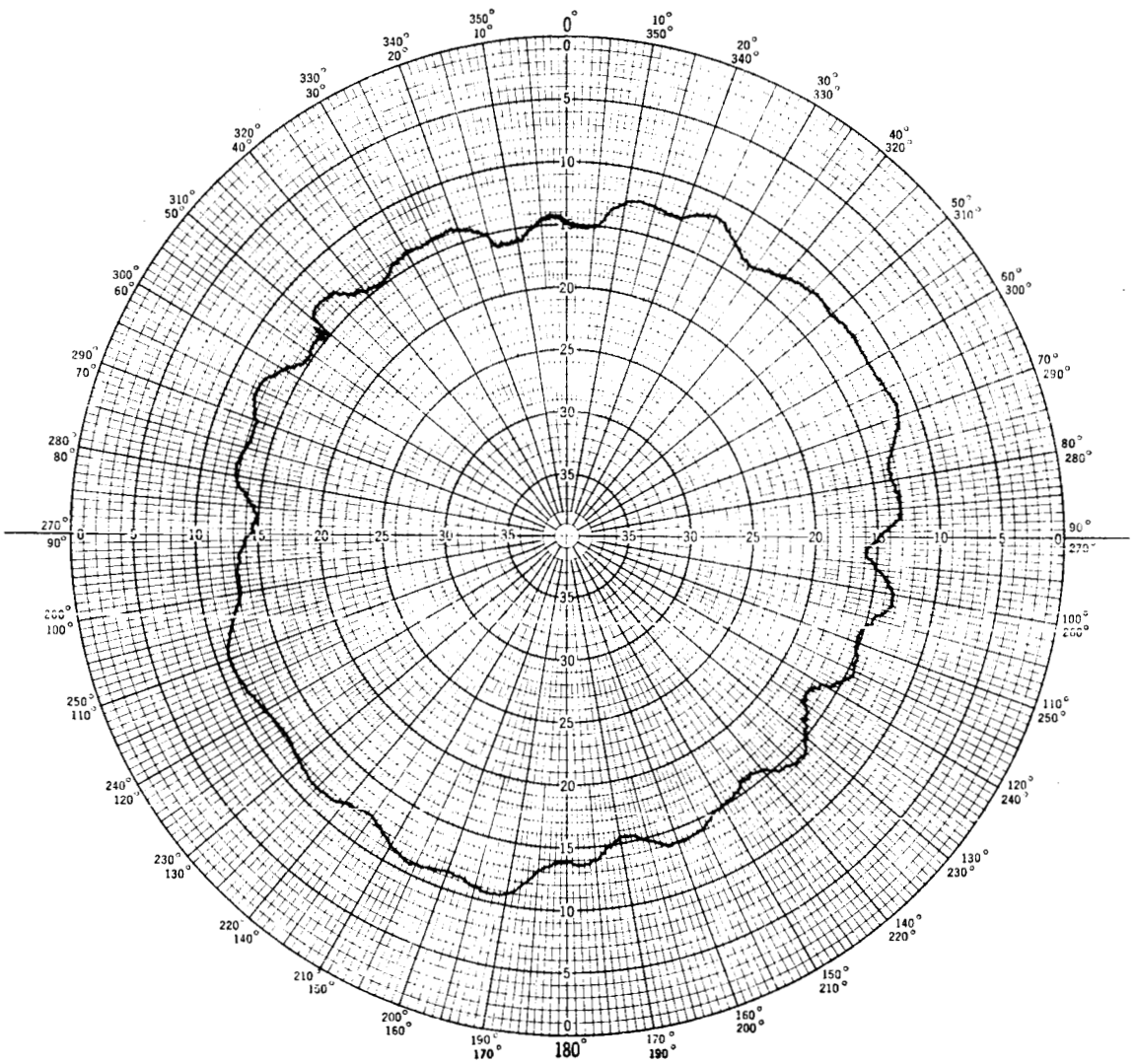

Fig. B-12--The Azimuth Pattern of the Rexolite Dielectric Loaded Crossed-Slot Antenna ($\theta = 55^{o}$)

Polar Chart No. 127D
SCIENTIFIC-ATLANTA, INC.
ATLANTA, GEORGIA

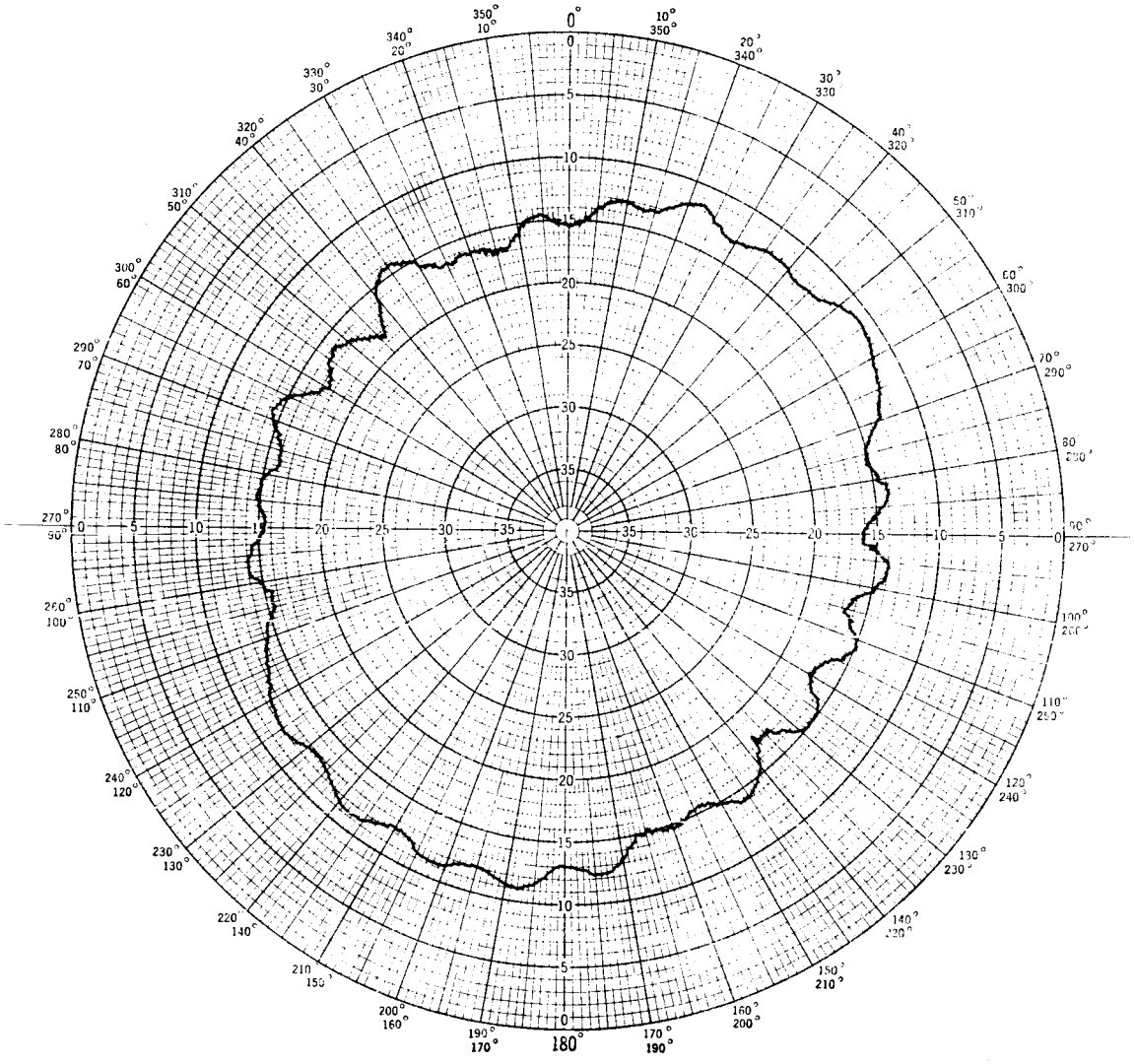

Fig. B-13--The Azimuth Pattern of the Rexolite Dielectric Loaded Crossed-Slot Antenna ($\theta = 60^{\circ}$)

Polar Chart No. 127D
SCIENTIFIC-ATLANTA, INC.
ATLANTA, GEORGIA

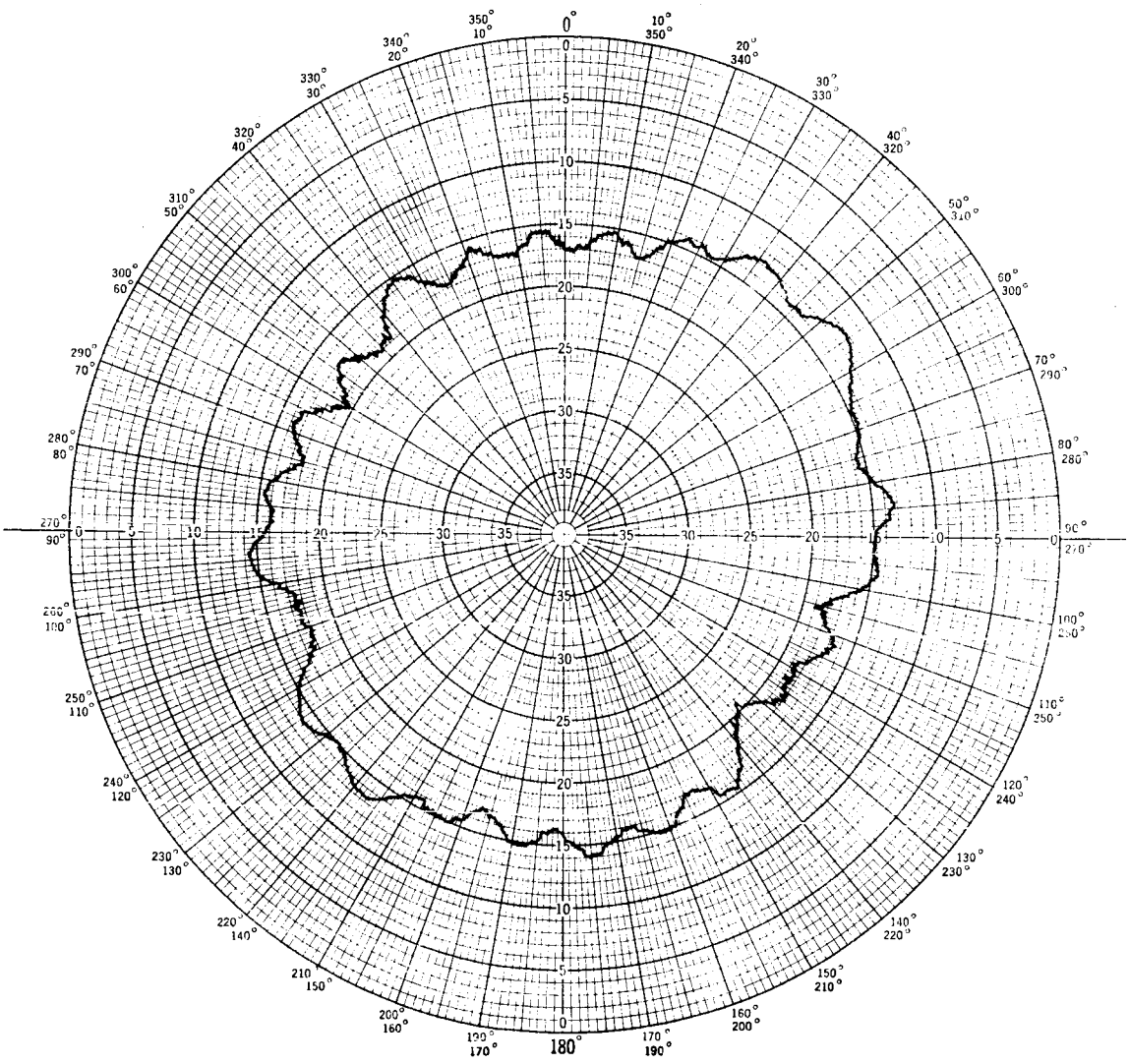

Fig. B-14--The Azimuth Pattern of the Rexolite Dielectric Loaded Crossed-Slot Antenna ($\theta = 65^{\circ}$)

Polar Chart No. 127D
SCIENTIFIC-ATLANTA, INC.
ATLANTA, GEORGIA

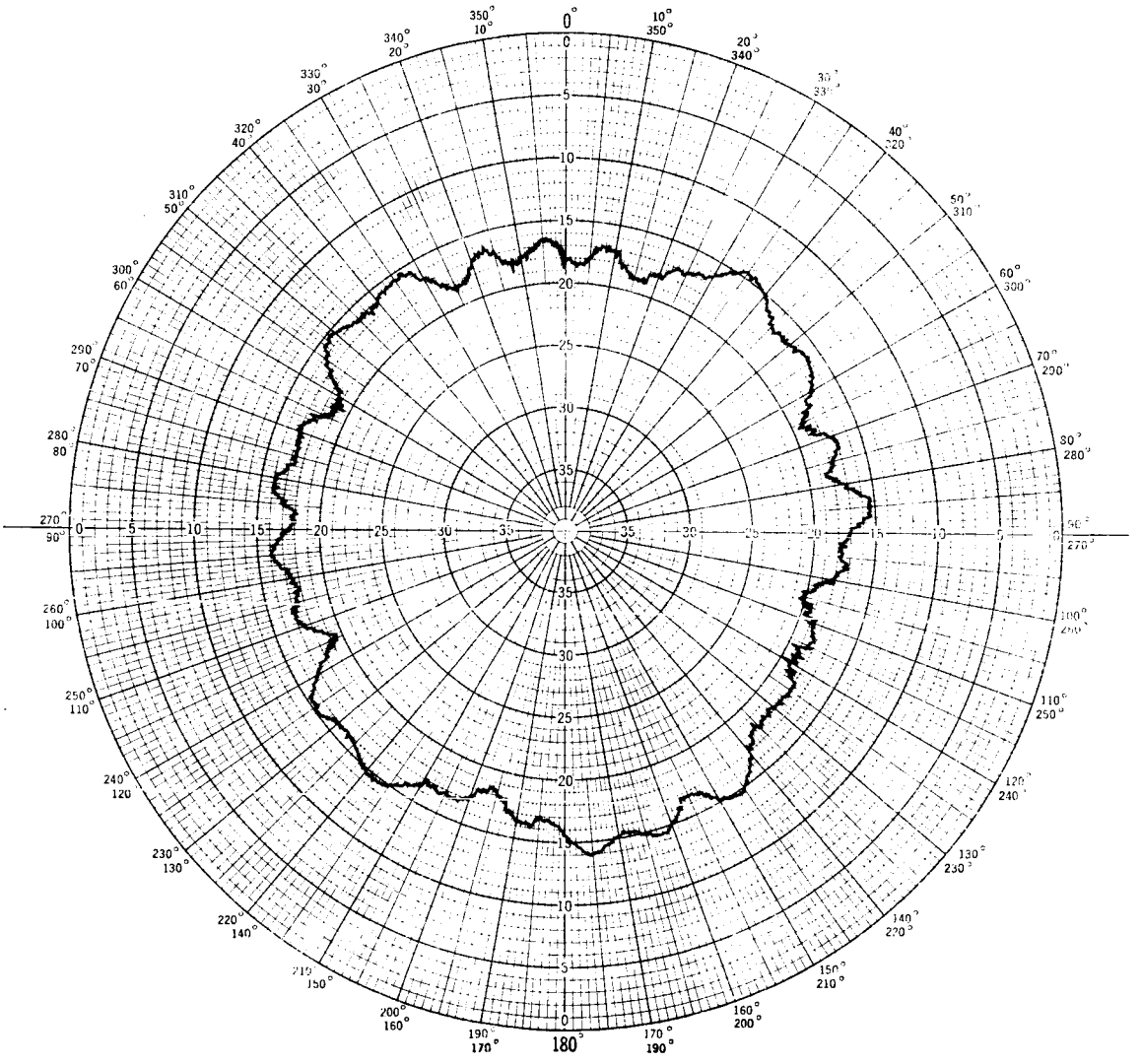

Fig. B-15--The Azimuth Pattern of the Rexolite Dielectric Loaded Crossed-Slot Antenna ($\theta = 70^{\circ}$)

Polar Chart No. 127D
SCIENTIFIC-ATLANTA, INC.
ATLANTA, GEORGIA

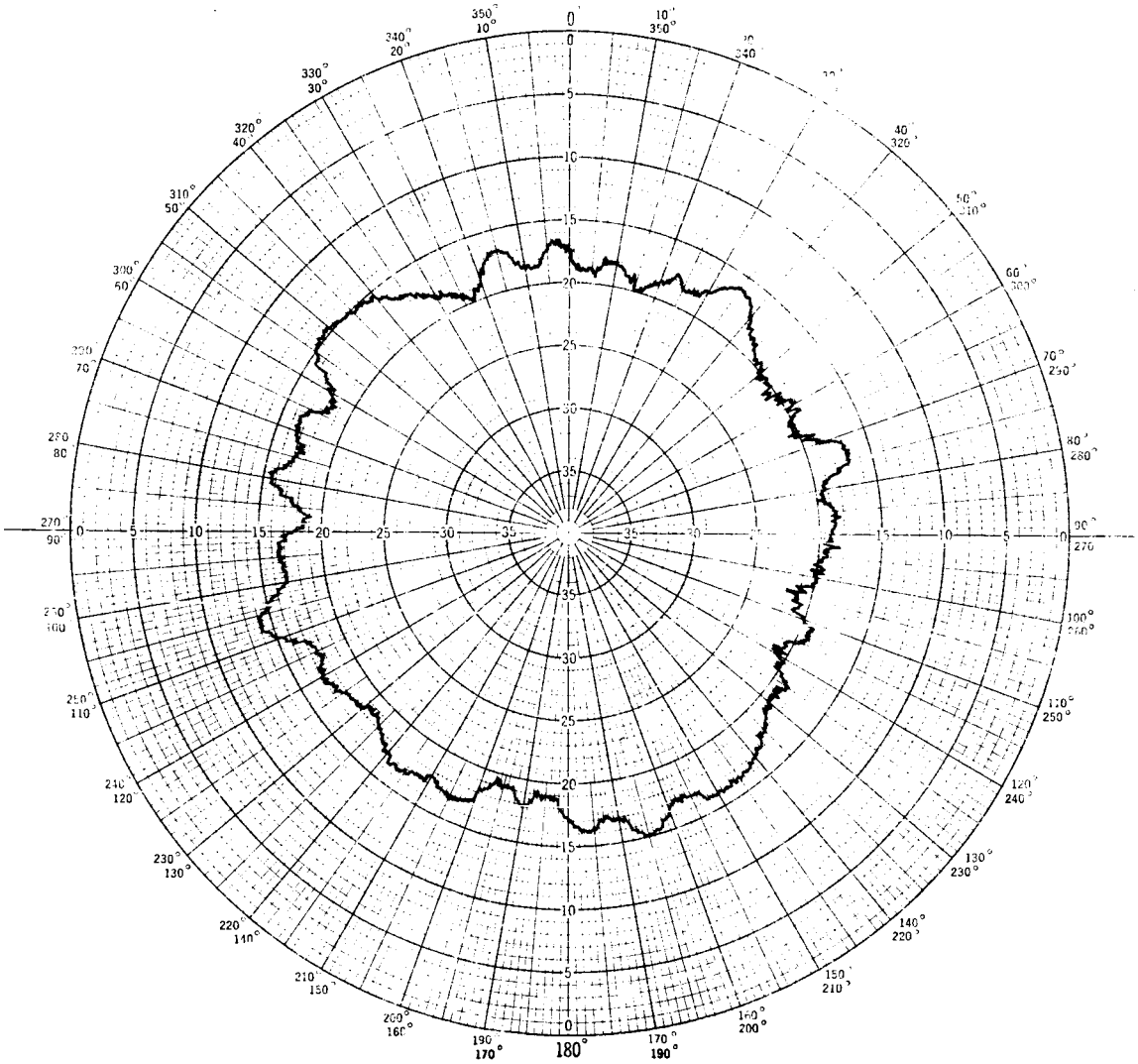

Fig. B-16--The Azimuth Pattern of the Rexolite Dielectric Loaded Crossed-Slot Antenna ($\theta = 75^{o}$)

Polar Chart No. 127D
SCIENTIFIC-ATLANTA, INC.
ATLANTA, GEORGIA

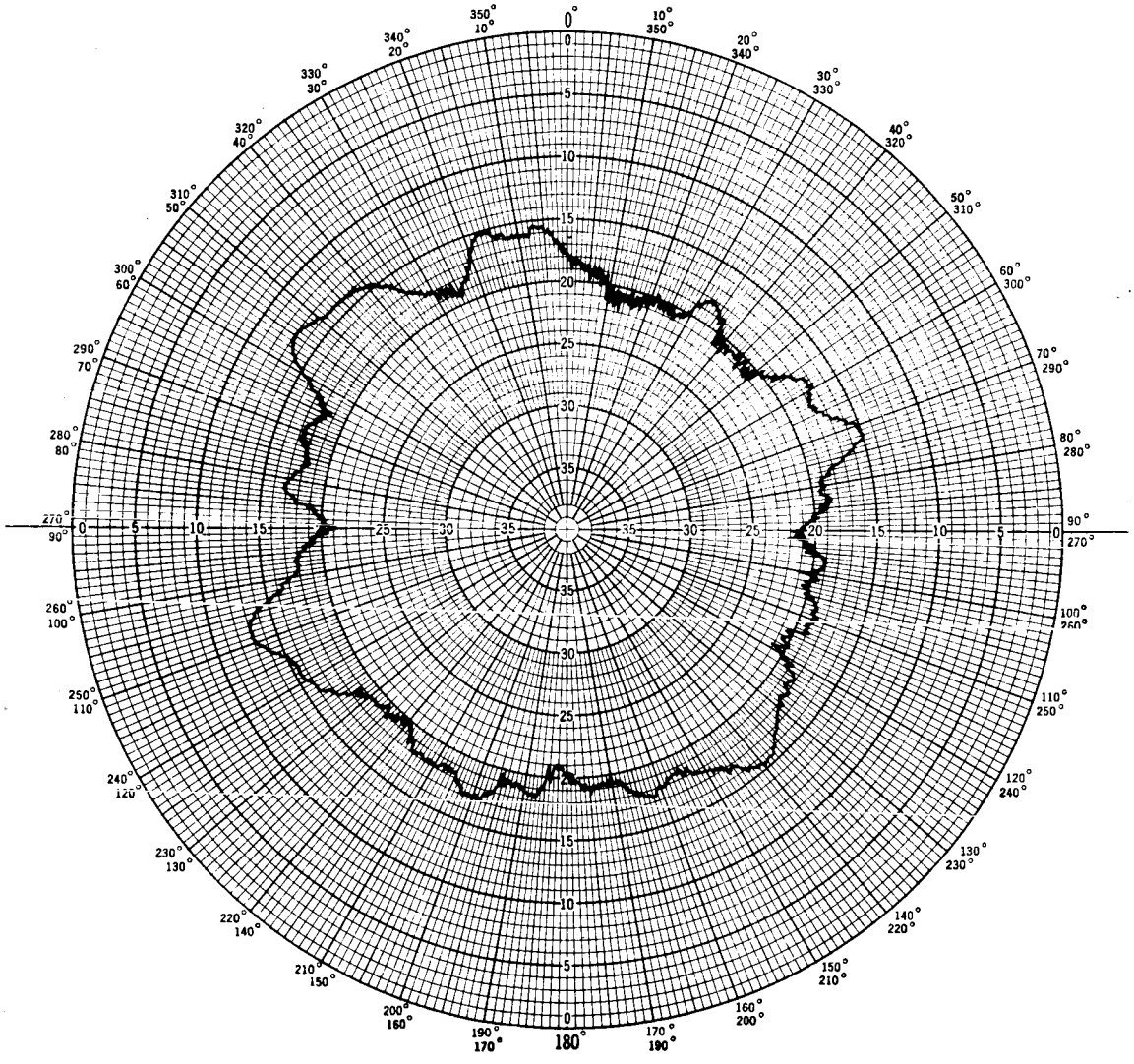

Fig. B-17--The Azimuth Pattern of the Rexolite Dielectric Loaded Crossed-Slot Antenna (θ = 80°)

Polar Chart No. 127D
SCIENTIFIC-ATLANTA, INC.
ATLANTA, GEORGIA

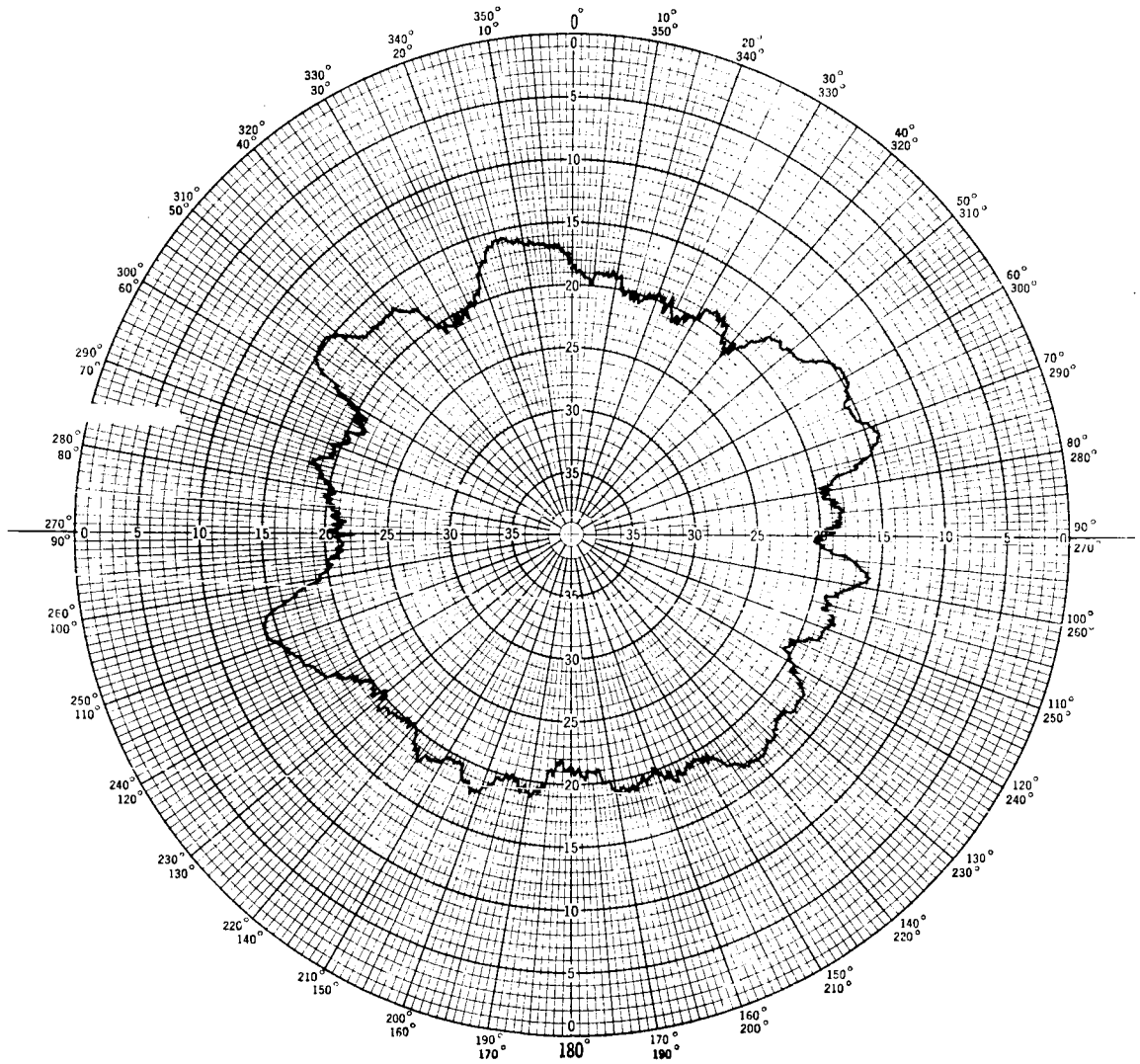

Fig. B-18--The Azimuth Pattern of the Rexolite Dielectric Loaded Crossed-Slot Antenna ($\theta = 85^{o}$)

Polar Chart No. 127D
SCIENTIFIC-ATLANTA, INC.
ATLANTA, GEORGIA

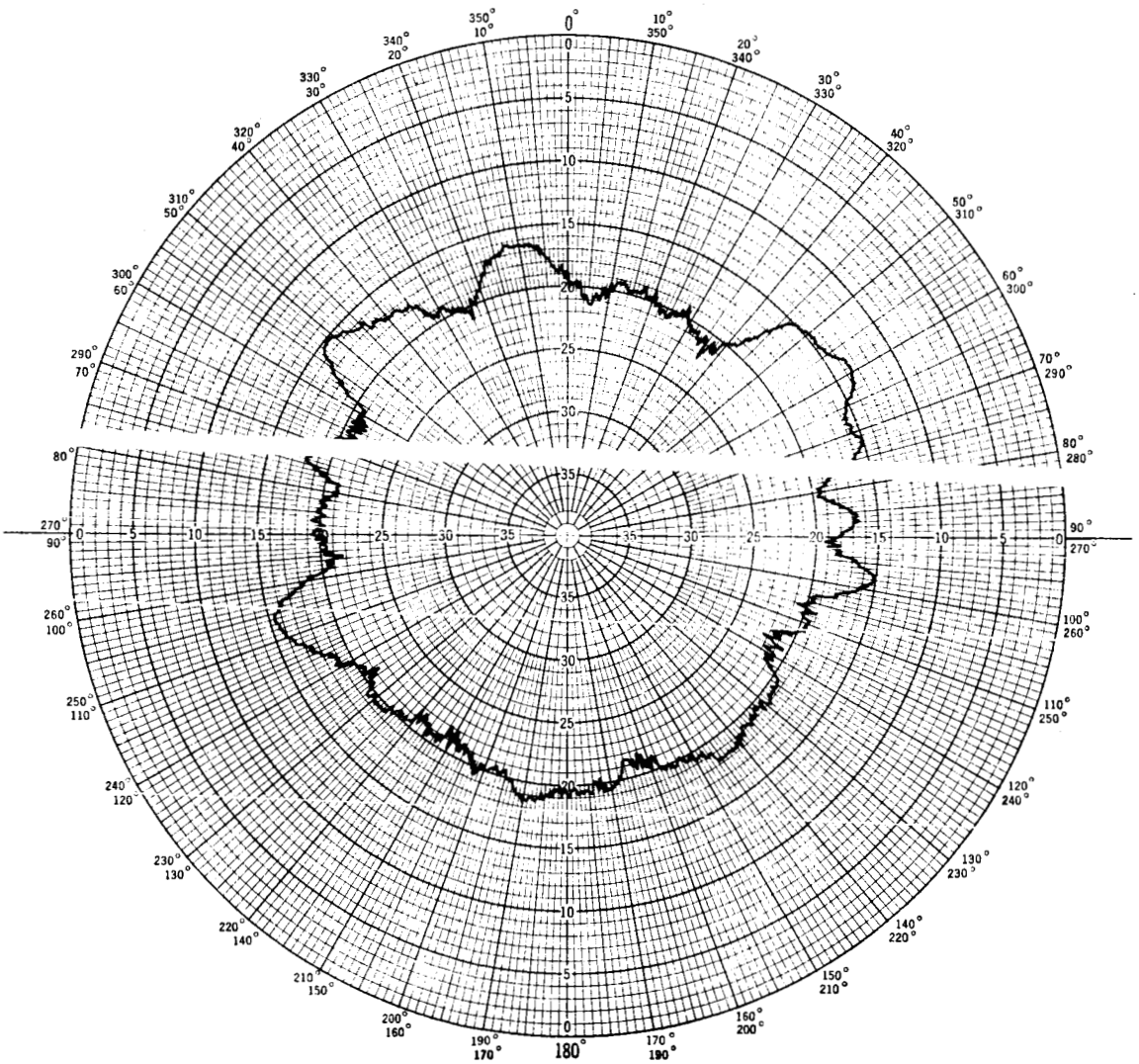

Fig. B-19--The Azimuth Pattern of the Rexolite Dielectric Loaded Crossed-Slot Antenna ($\Theta = 90^{o}$)

Polar Chart No. 127D
SCIENTIFIC-ATLANTA, INC.
ATLANTA, GEORGIA

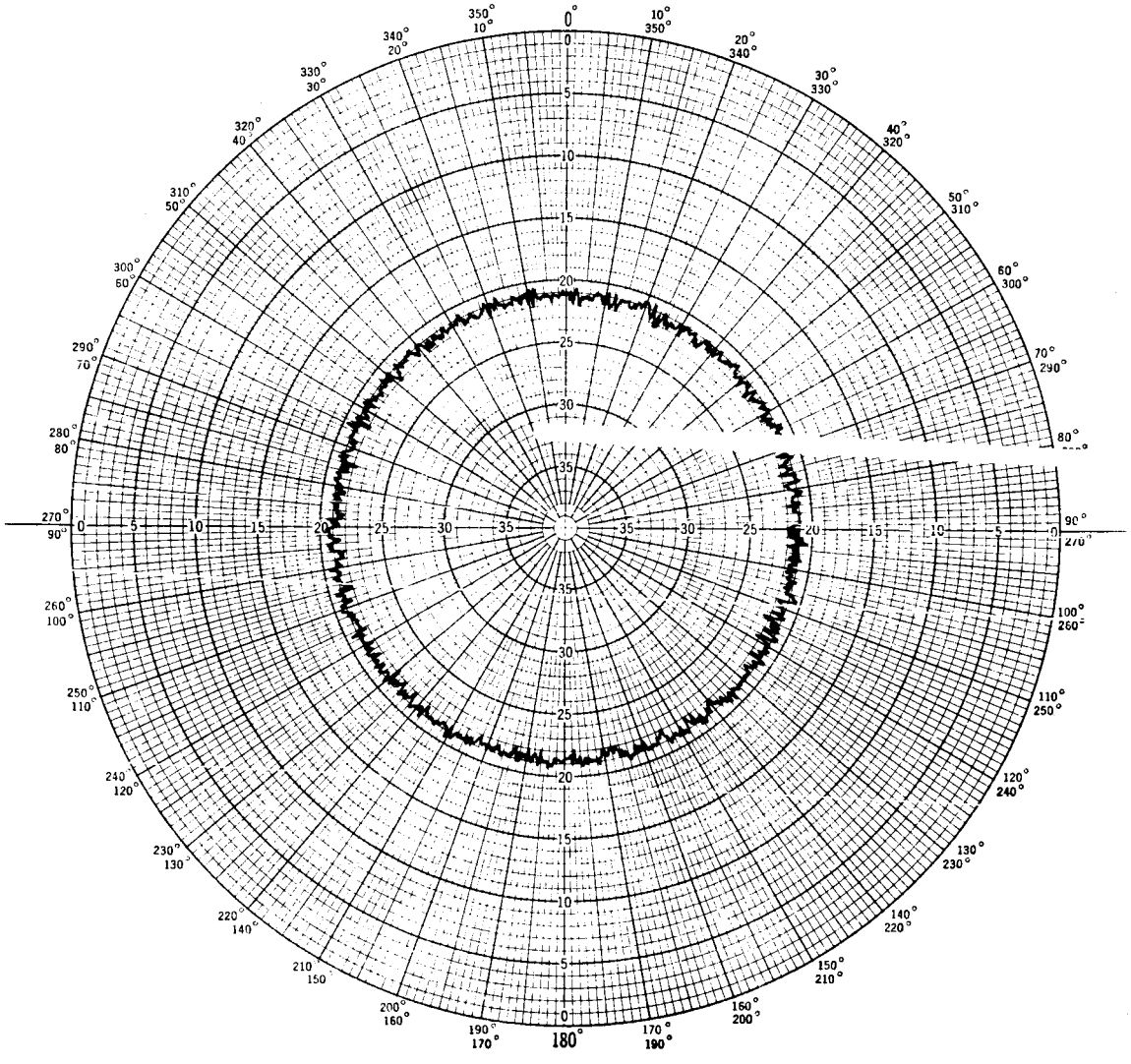

Fig. B-20--Receiver Noise Level for Azimuth Pattern Measurements

Polar Chart No. 127D
SCIENTIFIC-ATLANTA, INC.
ATLANTA, GEORGIA

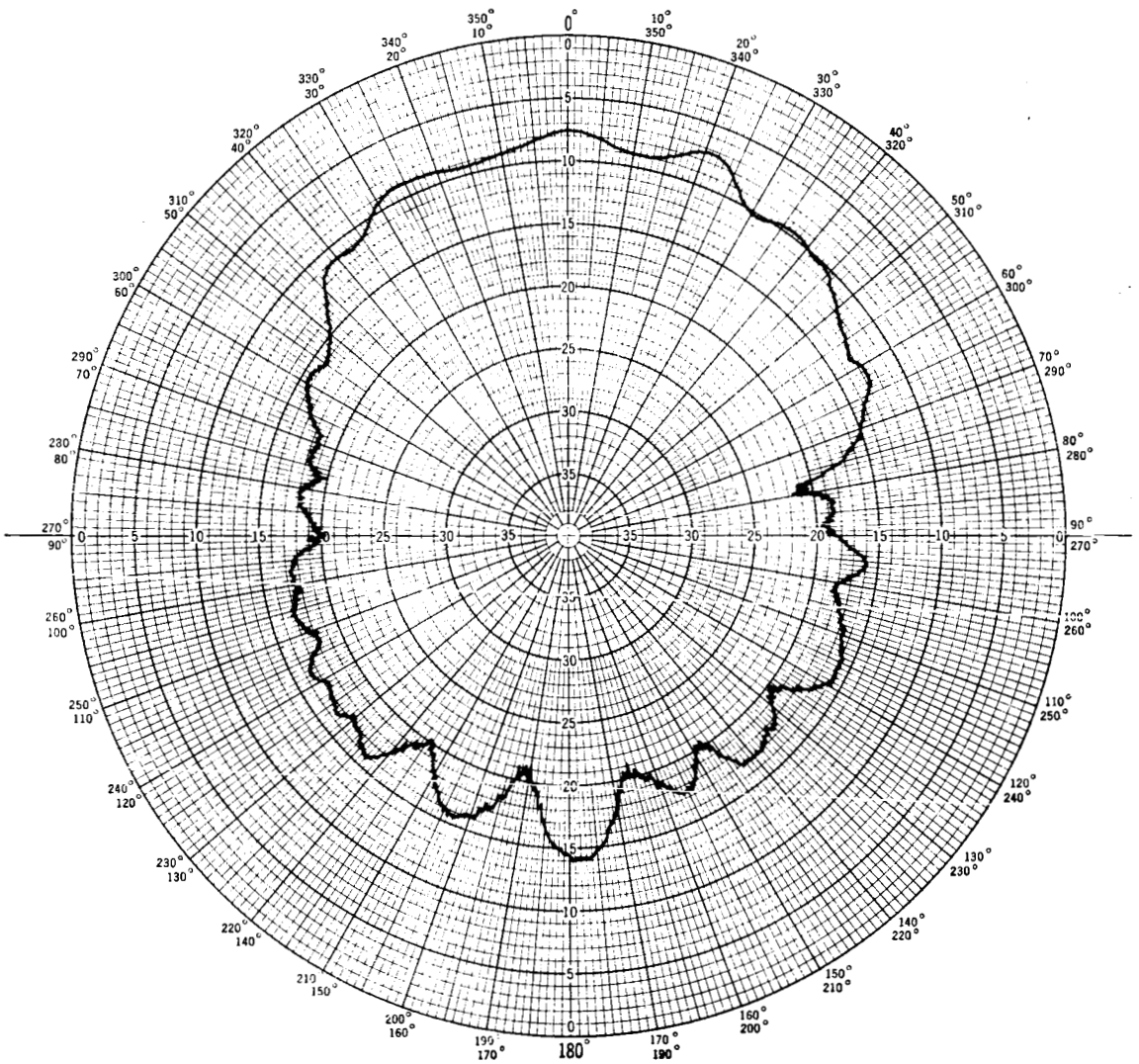

Fig. B-21--The Elevation Pattern of the Rexolite Dielectric Loaded Crossed-Slot Antenna Along the X-Axis Slot

Polar Chart No. 127D
SCIENTIFIC-ATLANTA, INC.
ATLANTA, GEORGIA

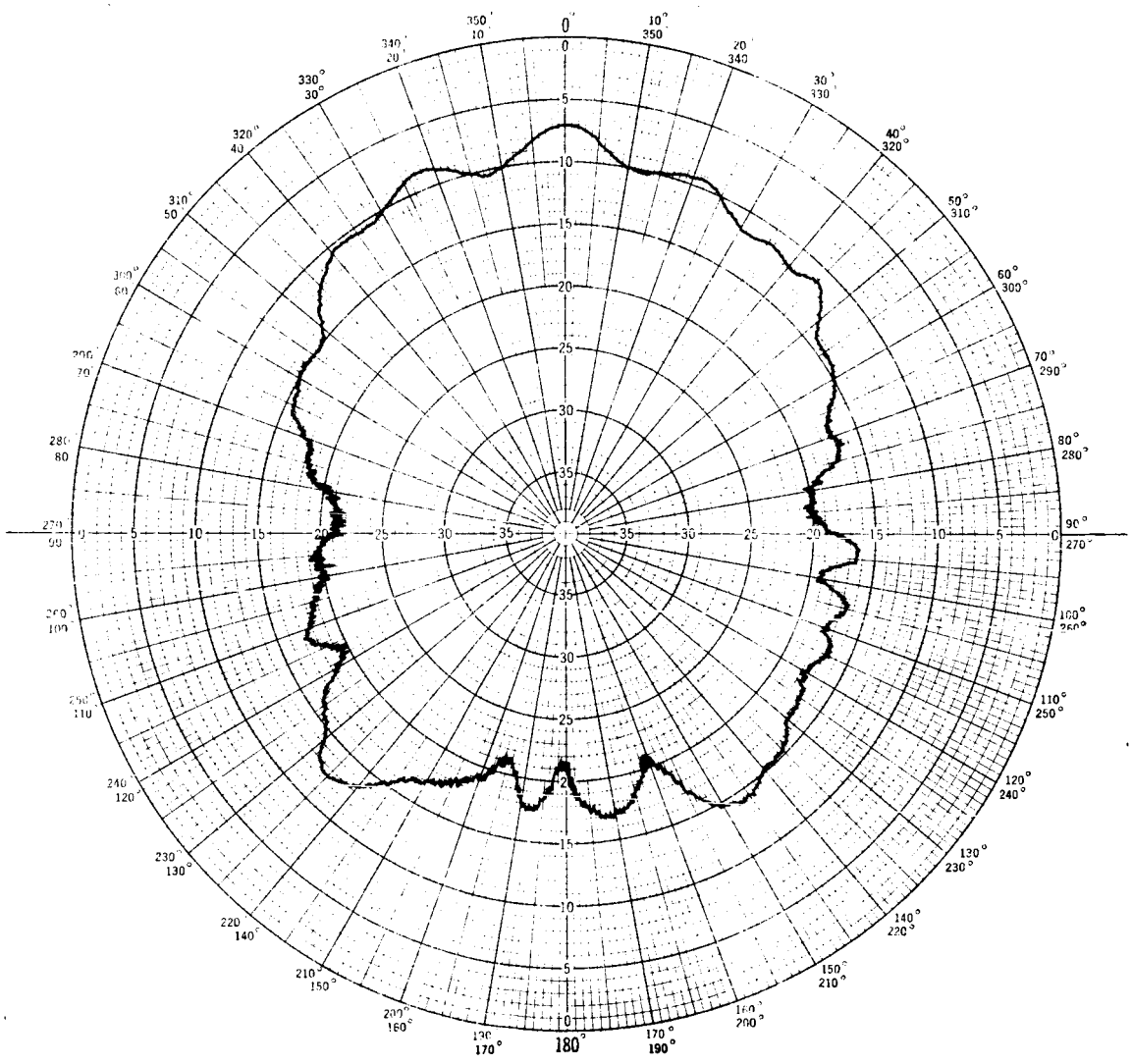

Fig. B-22--The Elevation Pattern of the Rexolite Dielectric Loaded Crossed-Slot Antenna Along the Y-Axis Slot

Polar Chart No. 127D
SCIENTIFIC-ATLANTA, INC.
ATLANTA, GEORGIA

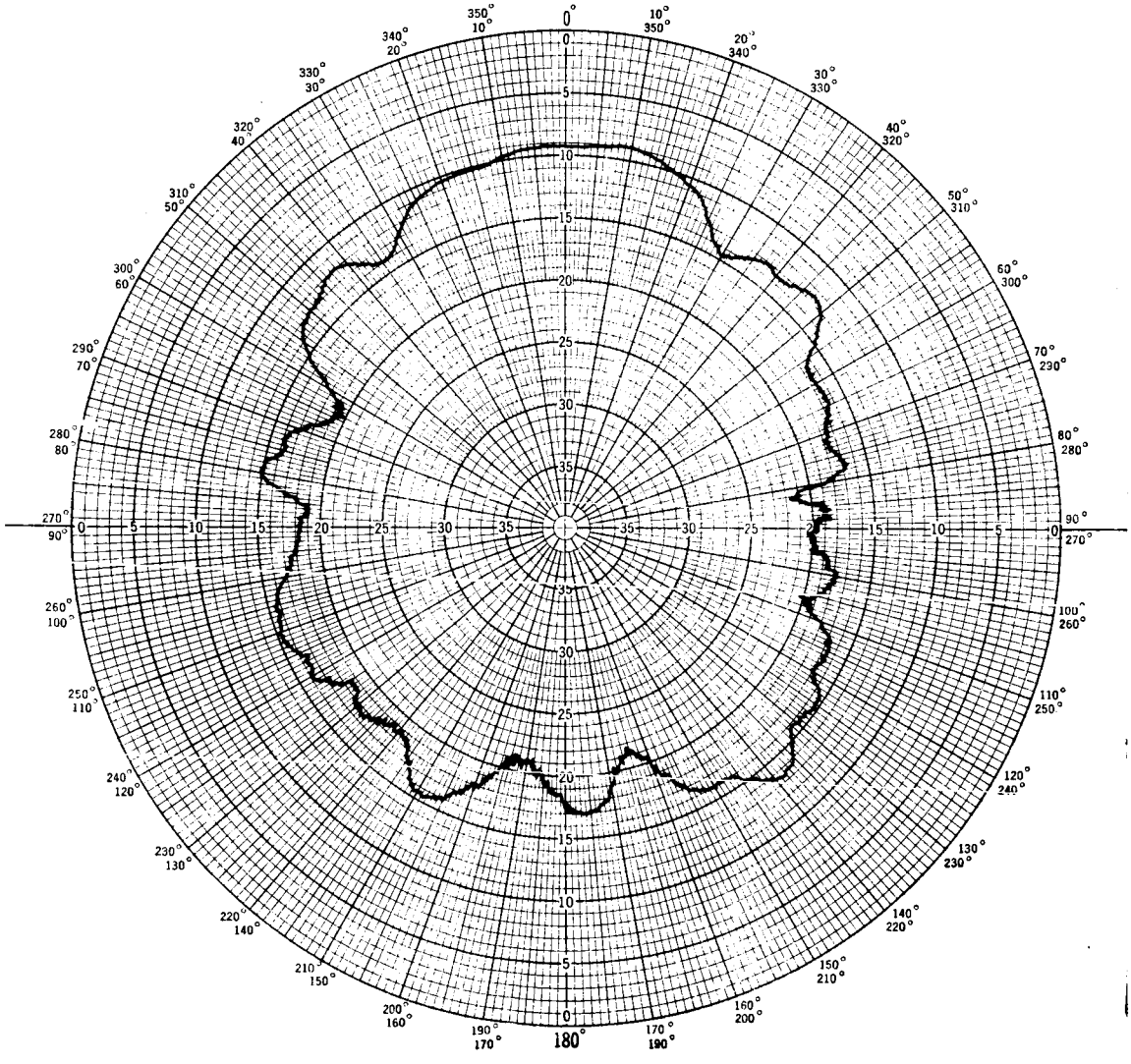

Fig. B-23--The Elevation Pattern of the Rexolite Dielectric Loaded Crossed-Slot Antenna Along the Plane of Minimum Variation ($\Phi = 45^{\circ}$)

Polar Chart No. 127D
SCIENTIFIC-ATLANTA, INC.
ATLANTA, GEORGIA